

Journal Pre-proof

Design, synthesis characterization and biological evaluation of novel multi-isoform ALDH inhibitors as potential anticancer agents

Saketh S. Dinavahi, Raghavendra Gowda, Christopher G. Bazewicz, Madhu Babu Battu, Jyh Ming Lin, Robert J. Christen, Manoj K. Pandey, Shantu Amin, Gavin P. Robertson, Krishne Gowda

PII: S0223-5234(19)31114-6

DOI: <https://doi.org/10.1016/j.ejmech.2019.111962>

Reference: EJMECH 111962

To appear in: *European Journal of Medicinal Chemistry*

Received Date: 11 September 2019

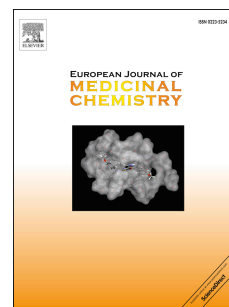
Revised Date: 3 December 2019

Accepted Date: 9 December 2019

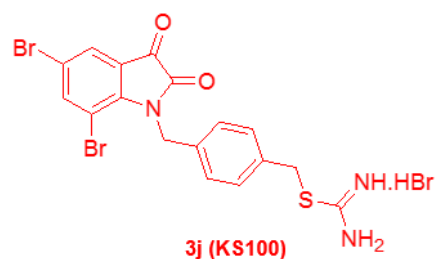
Please cite this article as: S.S. Dinavahi, R. Gowda, C.G. Bazewicz, M.B. Battu, J.M. Lin, R.J. Christen, M.K. Pandey, S. Amin, G.P. Robertson, K. Gowda, Design, synthesis characterization and biological evaluation of novel multi-isoform ALDH inhibitors as potential anticancer agents, *European Journal of Medicinal Chemistry* (2020), doi: <https://doi.org/10.1016/j.ejmech.2019.111962>.

This is a PDF file of an article that has undergone enhancements after acceptance, such as the addition of a cover page and metadata, and formatting for readability, but it is not yet the definitive version of record. This version will undergo additional copyediting, typesetting and review before it is published in its final form, but we are providing this version to give early visibility of the article. Please note that, during the production process, errors may be discovered which could affect the content, and all legal disclaimers that apply to the journal pertain.

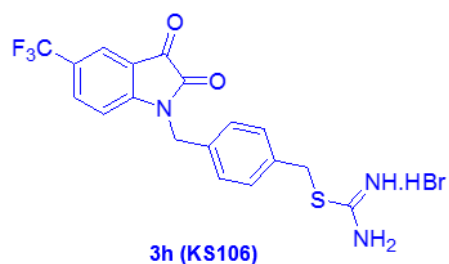
© 2019 Published by Elsevier Masson SAS.



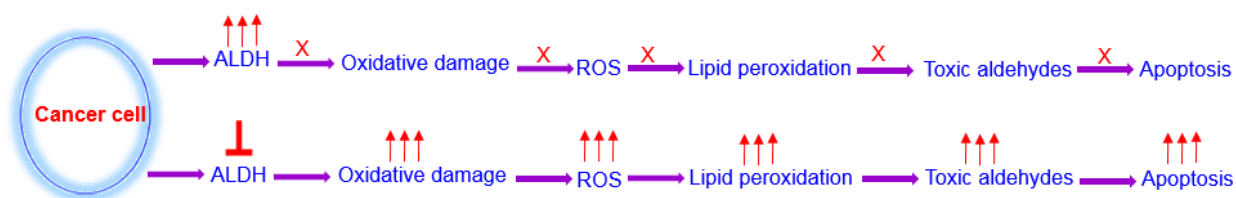
Graphical Abstract



ALDH Enzyme Inhibition (IC_{50s})
 ALDH1A1 = 230 nM
 ALDH2 = 1542 nM
 ALDH3A1 = 193 nM
 Potent, toxic



ALDH Enzyme Inhibition (IC_{50s})
 ALDH1A1 = 294 nM
 ALDH2 = 1795 nM
 ALDH3A1 = 260 nM
 Potent, non-toxic



Design, synthesis characterization and biological evaluation of novel multi- isoform ALDH inhibitors as potential anticancer agents

Saketh S. Dinavahi^{a,f}, Raghavendra Gowda^{a,f}, Christopher G. Bazewicz^{f,g}, Madhu Babu Battu^j, Jyh Ming Lin^e, Robert J. Christenⁱ, Manoj K. Pandeyⁱ, Shantu Amin^{a,h}, Gavin P. Robertson^{a,b,c,d,f}, Krishne Gowda^{a,h*}

^aDepartment of Pharmacology, ^bPathology, ^cDermatology, ^dSurgery, ^eBiochemistry and Molecular Biology, ^fMelanoma Skin Cancer Center, ^gCollege of Medicine, ^hPenn State Hershey Cancer Institute, The Pennsylvania State University College of Medicine, Hershey, PA 17033, United States; ⁱDepartment of Biomedical Sciences, Cooper Medical School of Rowan University, Camden, NJ 08103, United States; ^jLaboratory of Molecular Cell Biology, Centre for DNA Fingerprinting and Diagnostics, Uppal, Hyderabad, 500039, India.

***Corresponding author:** Krishne Gowda, Department of Pharmacology, The Pennsylvania State University College of Medicine, 500 University Drive, Hershey, PA 17033, United States. Phone: (717) 531-0003 Ext. 285014; Fax: (717) 531-0244; E-mail: kgowda@pennstatehealth.psu.edu

Funding sources: G.P.R. acknowledges the Penn State Chocolate Tour Cancer Research fund and Melanoma Research Alliance fund.

Short title: Novel multi-ALDH isoform inhibitors.

Word count: 6513

Key words: Aldehyde dehydrogenases, Cancer therapeutics, Colon cancer, Multiple Myeloma, Drug design, Drug development, Molecular docking.

Conflicts of interest: The authors declare no conflicts of interest.

Abstract

The aldehyde dehydrogenases (ALDHs) are a family of detoxifying enzymes that are overexpressed in various cancers. Increased expression of ALDH is associated with poor prognosis, stemness, and drug resistance. Because of the critical role of ALDH in cancer stem cells, several ALDH inhibitors have been developed. Nonetheless, all these inhibitors either lack efficacy or too toxic or not been tested extensively. Thus, the continued development of ALDH inhibitors is warranted. In this study, we designed and synthesized potent multi-ALDH isoform inhibitors based on the isatin backbone. The early molecular docking studies and enzymatic tests revealed that **3(a-l)** and **4(a-l)** are the potent ALDH1A1, ALDH2, and ALDH3A1 inhibitors. ALDH inhibitory IC₅₀s of **3(a-l)** and **4(a-l)** were 230 nM to >10,000 nM for ALDH1A1, 939 nM to >10,000 nM for ALDH2 and 193 nM to >10,000 nM for ALDH3A1. The most potent compounds **3(h-l)** had IC₅₀s for killing melanoma cells ranged from 2.1 to 5.7 μ M, while for colon cancer cells ranged from 2.5 to 5.8 μ M and for multiple myeloma cells ranged from 0.3 to 4.7 μ M. Toxicity studies of **3(h-l)** revealed that **3h** to be the least toxic multi-ALDH isoform inhibitor. Mechanistically, **3(h-l)** caused increased ROS activity, lipid peroxidation, and toxic aldehyde accumulation, secondary to potent multi-ALDH isoform inhibition leading to increased apoptosis and G2/M cell cycle arrest. Together, the study details the design, synthesis, and evaluation of potent, multi-isoform ALDH inhibitors to treat cancers.

1. Introduction

The human aldehyde dehydrogenases (ALDHs) are a family of 19 enzymes that oxidize endogenous and exogenous aldehydes to less reactive, more soluble carboxylic acids in a NAD(P)⁺-dependent reaction [1, 2]. The ALDHs protect cells against oxidative stress and reactive oxygen species (ROS), which trigger lipid peroxidation and the accumulation of toxic aldehydes, such as acrolein, malondialdehyde (MDA), 4-hydroxy-2-nonenal (4-HNE) and 4-hydroxy-2-hexanal (4-HHE) [3]. Collection of such aldehydes damages cells by forming protein adducts through non-enzymatic, covalent bonds with lysine, cysteine, and histidine residues, as well as through increased ROS generation and lipid peroxidation [3-5]. Consequently, cancer cells often overexpress ALDH isoforms to combat oxidative stress secondary to high metabolic demands, radiation, and ROS-generating chemotherapeutics, including paclitaxel, doxorubicin, staurosporine, and sorafenib [6].

Overexpression of ALDH isoforms is associated with cancer progression, resistance and poor prognosis in numerous cancers including breast, lung, colorectal, esophageal, Ewing's sarcoma, head and neck squamous cell carcinoma (HNSCC), melanoma, mesothelioma, multiple myeloma, neuroblastoma, prostate, and pancreatic cancer [7-18]. ALDH1A1 and ALDH3A1 directly metabolize the active metabolites of cyclophosphamide, contributing to resistance against this chemotherapeutic drug [19]. Cancer cells with a stem-cell-like phenotype, which are a small subset of multipotent cells within tumors responsible for tumor initiation, progression, resistance, and metastasis, often express high levels of ALDH [20, 21]. Further, retinoic acid generated by ALDH1A1, ALDH1A2, and ALDH1A3 can lead to the induction and function of tumor-infiltrating regulatory T cells, which create an immunosuppressive tumor microenvironment and impair tumor immunity [22].

Due to the role of ALDH overexpression in cancer progression and therapy resistance, many ALDH inhibitors have been developed [23]. Current ALDH inhibitors can be classified into multi-ALDH isoform inhibitors and isoform-specific inhibitors, which primarily inhibit one isoform [23]. Multi-ALDH isoform inhibitors include *N,N*-diethylaminobenzaldehyde (DEAB), 4-dimethylamino-4-methyl-pent-2-ynthioic acid-S-methylester (DIMATE), citral, ALDH inhibitors (aldis)-1, -2, -3, -4 and -6 and dyclonine [23-33]. Each inhibitor exhibits antiproliferative effects on cultured cancer cells, particularly as combinatorial therapy, but only DEAB, DIMATE, citral, aldi-6, and dyclonine have been tested in *in vivo* cancer models [23-33]. DEAB, DIMATE, citral, and aldi-6 show

antitumor efficacy as monotherapy; however, variations in ALDH expression hinder the efficacy of DEAB, the oral bioavailability of DIMATE has not been reported, and citral has a range of off-target effects leading to toxicity [24, 26-30, 32]. Aldi-6 at 24 mg/kg/day inhibits HNSCC xenograft development by 60% with no toxicity observed [32]. However, it was administered via an osmotic mini-pump, and due to its recent development, has not been tested further [32].

Isoform-specific ALDH inhibitors include the ALDH1A1 specific inhibitors Cpd 3, CM037, CM026, NCT-501, NCT-505, NCT-506, 13g and 13h, the ALDH2 specific inhibitor CVT10216, and the ALDH3A1 specific inhibitors CB7 and CB29 [23, 34-40]. Minimal *in vivo* data exist for these compounds, either due to limited efficacy, poor bioavailability, or recent development [23, 34-40]. NCT-501 has been tested *in vivo*, and leads to a 78% reduction in HNSCC xenograft growth; however, it was administered via intratumoral injection [36]. Thus, the development of novel, potent, non-toxic, bioavailable ALDH inhibitors is still needed [41]. Targeting more than one ALDH isoform is likely necessary for optimal anticancer therapy, as ALDH activity within cancer cells is generally a composite of the activity of multiple ALDH isoforms [1, 2, 41].

In the present study, a series of novel, potent, multi-ALDH isoform inhibitors were designed and synthesized. Ligand-based docking studies were used to identify **3(a-l)** and **4(a-l)**. **3(a-l)** and **4(a-l)** indicated strong docking scores for ALDH1A1, ALDH2, and ALDH3A1 and were subsequently synthesized and ALDH inhibitory activity evaluated. Compounds **3(h-l)** had the highest potency against ALDH1A1, ALDH2, and ALDH3A1 and showed efficacy and selectivity for killing cultured colon cancer, multiple myeloma, and melanoma cell lines. Toxicity in animals was significant for **3(i-l)**, whereas **3h** was not toxic. Thus, **3h** may be useful for the treatment of cancer.

Mechanistically, **3(h-l)** led to a significant increase in toxic aldehyde accumulation, ROS activity, and lipid peroxidation mediated by potent ALDH1A1, ALDH2, and ALDH3A1 inhibition leading to increased apoptosis and G2/M arrest of the cell cycle. N-acetyl cysteine (NAC), a ROS scavenger reduced the activity of the active compounds demonstrating the significance of ROS activity in ALDH pathway.

2. Results and Discussion

2.1. Molecular docking studies

Multi-ALDH isoform inhibition may be more useful for cancer treatment since ALDH activity within cancer cells is a composite of multiple ALDH isoforms [1, 2]. Cpd 3, an isatin analog, is one of the most potent ALDH1A1 specific inhibitors (**Fig. 1**) [34]. We have previously identified KS99 (**Fig. 1**), a similar isatin analog, to be a potent ALDH inhibitor to reduce cancer growth [42-44]. It exhibits multi-ALDH isoform inhibition with IC₅₀s of 350 nM, 1.5 μ M, and 850 nM for ALDH1A1, ALDH2, and ALDH3A1, respectively (unpublished data), but is toxic in animals starting at 5 mg/kg/day [44]. Thus, we attempted to optimize the structure of KS99 using molecular docking studies to develop novel, non-toxic, potent, multi-ALDH isoform inhibitors.

A series of compounds **3(a-l)** and **4(a-l)** were designed and tested for the ability to bind in the active site pockets of ALDH1A1, ALDH2, and ALDH3A1 using molecular docking studies. 1,4-bis(bromomethyl) benzene was selected as a linker to connect the isatin scaffold and isothioureia moieties. The protein structures of ALDH1A1, ALDH2, and ALDH3A1 co-crystallized with the corresponding potent, isoform-specific ALDH inhibitors CM037 (ALDH1A1), psoralen (ALDH2) and CB7 (ALDH3A1) were selected. The designed compounds were first docked into the ligand-binding pocket of ALDH1A1. Significant interactions identified between the crystal ligand, CM037, and ALDH1A1 were a π - π interaction with the W178 residue and an H-bond interactions with the Gly458 and Ser121 residues along with interactions with Cys303. Isatin did not exhibit any of these interactions with ALDH1A1; however, KS99 had a similar π - π interaction with the W178 residue and H-bond interactions with the Gly458 and Ser121 residues of ALDH1A1. Cpd 3 had interactions with W178 and S121. Importantly, compounds **3(a-l)** and **4(a-l)** shared similar interactions (**Fig. 2** and **Fig. S1**) with residues in the ligand-binding pocket of ALDH1A1 compared to CM037 and KS99, suggesting they could potentially be inhibitors of ALDH1A1.

Docking studies were similarly conducted with compounds and the ALDH2 and ALDH3A1 protein structures. π - π interactions with the F459 residue and H-bond interactions with the L269 residues occurred between ALDH2 and the crystal ligand, psoralen. Similarly, π - π interactions with the T115 residue occurred between ALDH3A1 and the crystal ligand, CB7. Importantly, compounds **3(a-l)** and **4(a-l)** shared similar interactions with residues in the ligand-binding pockets of ALDH2 and ALDH3A1 compared to psoralen and CB7, respectively (**Fig. 2** and **Fig. S1**), suggesting they could

be inhibitors of ALDH2 and ALDH3A1. As Cpd 3 is not an inhibitor of ALDH2 and ALDH3A1, it did not have these interactions. Docking scores for **3(a-l)** and **4(a-l)** ranged from -7.495 to -11.938 for ALDH1A1, -6.756 to -11.205 for ALDH2 and -12.119 to -14.564 for ALDH3A1 (**Table 1**). Based on these strong docking scores, **3(a-l)** and **4(a-l)** were synthesized for further analysis of ALDH enzyme inhibitory activity, anticancer efficacy, and toxicity.

2.2. Chemistry

The synthesis of target compounds, substituted 2-[4-(2,3-dioxo-2,3-dihydroindol-1-ylmethyl)benzyl]isothioureia hydrobromides **3(a-l)** and 2-[4-(2,3-dioxo-2,3-dihydroindol-1-ylmethyl)benzyl]isoselenourea hydrobromide analogs **4(a-l)** are illustrated in **Scheme 1**. The key intermediates **2(a-l)** were prepared in one step. Initially, unsubstituted, 5 or 7 mono substituted, and 5,7-disubstituted isatins were reacted with 1,4-bis(bromomethyl)benzene in the presence of potassium carbonate in DMF to the corresponding *N*-(*p*-bromomethylbenzyl) isatins **2(a-l)** in a good yield. These intermediates **2(a-l)** were then refluxed with thiourea in ethanol to produce the corresponding 2-[4-(2,3-dioxo-2,3-dihydroindol-1-ylmethyl)benzyl]isothioureia hydrobromides **3(a-l)** and refluxed with selenourea in ethanol to yield 2-[4-(2,3-dioxo-2,3-dihydroindol-1-ylmethyl)benzyl]isoselenourea hydrobromide analogs **4(a-l)** in an excellent yield. The structures of all isatin derivatives were confirmed by ¹H NMR, ¹³C NMR, and HRMS analysis. The compound purity (≥98%) was confirmed by analytical high-performance liquid chromatography (HPLC) before proceeding for *in vitro* biological assays.

2.3. ALDH isoform inhibitory activity

All the synthesized compounds **3(a-l)** and **4(a-l)** were assessed for the inhibition of ALDH1A1, ALDH2, and ALDH3A1 enzyme activity at various concentrations, and the results were summarized in **Table 2**. The enzymes inhibition were evaluated by measuring the conversion of NAD⁺ to NADH following the addition of isoform-specific aldehydes in the presence of **3(a-l)** and **4(a-l)**. ALDH inhibitory IC₅₀s activity of **3(a-l)** and **4(a-l)** were 230 nM to >10,000 nM for ALDH1A1, 939 nM to >10,000 nM for ALDH2 and 193 nM to >10,000 nM for ALDH3A1. (**Table 2**; dose-response curves in **Fig. S2**). **3(h-l)**, **4b**, and **4(j-l)** had the most potent inhibition of ALDH1A1, ALDH2, and ALDH3A1 at the concentrations tested and were considered potent, multi-ALDH isoform inhibitors. The most potent multi-ALDH isoform inhibitor, on average, was **3j**, which had IC₅₀s of 230 nM, 1542 nM, and 193 nM for ALDH1A1, ALDH2, and ALDH3A1 enzyme activity (**Table 2**).

Several trends in the structure-activity relationship of compounds **3(a-l)** and **4(a-l)** were noted (**Tables 1 and 2**). Compounds (X=S, series 3) with isothioureia moiety generally had greater multi-ALDH isoform inhibitory activity than that of corresponding isoselenourea compounds (X=Se, series 4). The lower inhibitory activity of selenium analogs may vary due to the larger size of selenium than a sulfur atom, which may interfere with the binding in the active-site pocket. For instance, **3h** and **3j** were more potent ALDH inhibitors than **4h** and **4j**, respectively. ALDH inhibitory activity of **3(a-l)** and **4(a-l)** depended on the halogen substitution at R₁ and/or R₂. Specifically, -dibromo substitutions (**3j**, **4j**) led to the best ALDH inhibition, followed by -dichloro (**3k**, **4k**), -fluoro, bromo (**3l**, **4l**), trifluoromethyl (**3h**), -fluoro (**3f**, **4f**) and finally un-substituted (**3a**, **4a**) compounds. Also, 5,7-disubstituted compounds (**3j**, **3k**) were more effective compared to 5-substituted (**3b**, **3d**) or 7-substituted (**3c**, **3e**) compounds. Further, 7-substituted compounds (**3c**, **3e**) were more effective than 5-substituted compounds (**3b**, **3d**). Finally, 5,7-dibromo substitutions (**3j**, **4j**) had greater ALDH inhibitory activity compared to 5-fluoro,7-bromo substitutions (**3l**, **4l**). Among all the compounds, 5,7-dibromo substitutions ultimately had the best ALDH inhibitory activity, may be due to larger size of bromine compared to other halogens and more hydrophobic nature of bromine, which facilitated the interaction in the hydrophobic binding pocket.

2.4. Cellular activity

Since isothioureia compounds (series 3) were in general, more potent ALDH1A1, ALDH2, and ALDH3A1 inhibitors compared to the corresponding isoseleno analogs (series 4), only **3(h-l)**, the most potent inhibitors in series 3, were tested for antiproliferative effects on cultured cancer cells. Specifically, **3(h-l)** were evaluated for inhibition of proliferation of cultured melanoma cells (UACC 903 and 1205 Lu) as ALDH overexpression is important in melanoma progression [45, 46]. The range of IC₅₀s against UACC 903 cells was 3 to 5.7 μ M, and for 1205 Lu cells was 2.1 to 5.7 μ M (**Table 3**; dose-response curves in **Fig. S3**), with **3j** and **3k** being the most effective across both cell lines. Cell killing by **3(h-l)** was also specific for melanoma cells compared to normal human fibroblasts (FF2441). Specifically, **3(h-l)** were 2- to 3.8-fold more selective for killing melanoma cells (**Table 3**). Importantly, **Cpd 3** and the inactive compound **3a** had IC₅₀s greater than 100 μ M in all the cell lines evaluated, demonstrating the importance of substitutions on the isatin ring of the compounds synthesized.

Subsequently, **3(h-l)** were evaluated for antiproliferative effects in several cancer types. Colon cancer cells (HCT116 and HT29) were studied as ALDH overexpression is also crucial in colon cancer progression [11, 47, 48]. Average IC₅₀s for each compound across both cell lines were 5.3 μ M for **3h**, 5.15 μ M for **3i**, 2.7 μ M for **3j**, 2.9 μ M for **3k** and 5.1 μ M for **3l** (**Table 3**; dose-response curves in **Fig. S3**). Compounds **3j** and **3k** were most effective in inhibiting the colon cancer cell survival likely due to their strong inhibition of ALDH1A1 and ALDH3A1. Multiple myeloma cells were also examined, as ALDH1A1 overexpression has been associated with stemness, therapy resistance, and poor outcomes in this cancer type [10, 49-52]. Average IC₅₀s for **3(h-l)** across all multiple myeloma cell lines tested (NCIH929, U266, RPMI8226, MM.1R, MM.1S) were 1.9 μ M for **3h**, 3.8 μ M for **3i**, 1 μ M for **3j**, 1.6 μ M for **3k** and 2.4 μ M for **3l** (**Table 3**; dose-response curves in **Fig. S4**). Compounds **3h**, **3j**, and **3k** showed more potent growth inhibition of multiple myeloma cells when compared to melanoma and colon cancer cells, demonstrating the more effectiveness of these compounds even in hematological malignancies. Additionally, these compounds displayed better IC₅₀s at killing melanoma cell with time, and IC₅₀s of **3j** were 7.2 μ M at 24 hours compared to 4.1 μ M at 48 hours and 3.7 μ M at 72 hours (**Fig. S5**). Thus, **3(h-l)** were specific to cancer cells and displayed antiproliferative activity against cultured melanoma, colon cancer, and multiple myeloma cells, indicating the potential for these compounds to be translated into the clinic. Moreover, **3(h-l)** displayed chemical properties predictive of good solubility, absorption, metabolism, and excretion (**Table 4**), indicating the drug-like properties of these compounds. All these compounds adhered to Lipinski's rule of five for drug-like compounds.

2.5. Toxicity studies

Since compounds **3(h-l)** were identified to be potent, multi-ALDH isoform inhibitors with antiproliferative activity in multiple cancer types, the toxicity of these compounds were evaluated for translatability to the clinic. Previously, we identified that KS99 was toxic in animals at 5 mg/kg/day [44]. Based on this data, we selected 5 mg/kg/day dose for the toxicity study with **3(h-l)** compounds. Specially, Swiss-Webster mice were treated with 5 mg/kg/day of **3(h-l)** i.p. for 14 days, and animal weight was compared to vehicle controls (**Table 5**). Compounds **3(i-l)** led to significant weight loss (10-15% body weight) after 14 days of treatment, while **3h** led to no significant weight loss (toxicity timeline in **Fig. S6**). Thus, **3h** was identified to be the least toxic agent, which may be due to lesser

ALDH inhibitory activity when compared to compounds **3(i-l)**. Toxicity of **3(i-l)** could be mitigated using controlled release formulations such as nanoliposomes [53].

2.6. ROS and lipid peroxidation activity and toxic aldehyde accumulation

Accumulation of toxic aldehydes (e.g., 4-HNE, 4-HHE, MDA, acrolein) secondary to ALDH inhibition can lead to protein adduct formation, increased ROS levels and lipid peroxidation, ultimately causing cell damage and apoptosis [3-5]. Thus, to evaluate the mechanism by which the ALDH inhibitors killed the cultured cancer cells, a ROS assay was performed using DCFDA dye [54]. Specifically, colon cancer cells, HCT116 and SW480 were treated with 5 μ M of the most potent ALDH inhibitor identified, compounds **3j** and the least toxic **3h** for 24 hours and ROS activity in treated cells was compared to DMSO. An inactive molecule in the series, **3a** was also included as a negative control, and H₂O₂ was used as a positive control. As shown in **Figure 3A** and **3B**, compounds **3h** and **3j** significantly increased ROS levels in both colon cell lines, indicating elevated ROS levels likely contribute to their anti-proliferative effects. Additionally, compound **3a**, an inactive derivative, did not significantly increase the ROS activity in any of the cell lines evaluated. Importantly, the ROS-inducing activity of compounds **3h** and **3j** was abrogated by the addition of N-Acetyl Cysteine (NAC), a scavenger of ROS activity in cells, indicating that the compounds affect the ROS-pathway.

To evaluate if **3h** and **3j** led to increased lipid peroxidation and toxic aldehyde accumulation, a lipid peroxidation assay was performed using a TBARS assay kit [55]. Specifically, HCT116 cells were treated with 5 μ M of **3h** and **3j** for 24 hours, and lipid peroxidation activity and toxic aldehyde accumulation in treated cells were compared to DMSO. As shown in **Figure 3C**, compounds **3h** and **3j** significantly increased lipid peroxidation and toxic aldehyde accumulation in HCT116 colon cancer cell line, likely contributing to their anti-proliferative effects. Additionally, **3a** was ineffective in increasing the lipid peroxidation; while the addition of NAC abrogated the effects of **3h** and **3j**, indicating the importance of ROS pathway in the accumulation of toxic aldehydes by these ALDH inhibitors.

Further, the effect of the addition of NAC on the anti-proliferative and apoptotic activity of ALDH inhibitors was also evaluated. Addition of NAC increased the cell killing IC₅₀s of **3h** and **3j** in colon cancer cell line, HCT116 by 6-fold, and 8-fold, respectively (**Fig. 3D**). Similar activity was observed in apoptosis and cell cycle assays where NAC abrogated the activity of the potent ALDH

inhibitors. When HCT116 colon cancer cells were treated with **3h** and **3j** at 5 μ M for 24 hours, the percentage of cells which are both Annexin-V and 7-AAD positive were significantly higher than the DMSO control-treated cells or inactive compound, **3a** treated cells (**Fig. 3E**; representative dot plots in **Fig. S7**). When NAC was added to these compounds, there was no increase in apoptotic cells compared to DMSO treated cells. Similarly, compounds **3j** and **3h** caused a G2/M arrest in the cell cycle activity of the colon cancer cell line HCT116, which was truncated by addition of NAC (**Fig. 3F**; representative histograms in **Fig. S8**). These data suggest that the potent ALDH inhibitors induce ROS activity, lipid peroxidation and accumulation of toxic aldehydes to inhibit cell survival and induce apoptosis through the modulation of ROS pathway.

3. Conclusion

In summary, this report details the design and synthesis of a series of novel, potent, multi-isoform ALDH inhibitors. Compounds with the best multi-ALDH isoform inhibition **3(h-l)** were evaluated for antiproliferative effects in multiple cancer types and displayed efficacy and selectivity for cultured cancer cells. Compound **3h** was not toxic in animals and thus may be the most promising anticancer drug in this study. Compounds **3(i-l)** were toxic, however, nanoliposomal formulations of **3(i-l)** could be developed to improve toxicity profiles as well as bioavailability. Mechanistically, potent multi-isoform ALDH inhibition led to significantly increased ROS activity, lipid peroxidation, and toxic aldehyde accumulation.

4. Experimental

4.1. Chemistry

4.1.1. General methods and materials

Isatin was purchased from Sigma-Aldrich (Sigma-Aldrich, St. Louis, MO, USA), 5,7-dibromo isatin was synthesized using previously reported methods [42]. Other chemicals were purchased from commercial vendors. Anhydrous solvents were used for all experiments. Reactions were carried out using dried glassware and under an atmosphere of nitrogen. Reaction progress was monitored with analytical thin-layer chromatography (TLC) on aluminum-backed precoated silica gel 60 F254 plates (E. Merck). The *N*-benzylisatins were highly colored and would usually be seen on a TLC plate; colorless compounds were detected using UV light and/or iodine vapor. Column chromatography was carried out using silica gel 60 (230–400 mesh, E. Merck) with the solvent system indicated in

the individual procedures. NMR spectra were recorded using a Bruker Avance II 500 or 600 MHz spectrometers. Chemical shifts (δ) were reported in parts per million downfield from the internal standard. The signals are quoted as s (singlet), d (doublet), t (triplet), m (multiplet), dd (doublet of doublet), ddd (doublet of doublets of doublets), dt (doublet of triplets). Spectra are referenced to the residual solvent peak of the solvent stated in the individual procedure. High-resolution mass spectra (HRMS) were determined in 5600 (QTOF) TripleTOF using a DuosprayTM ion source (Sciex, Framingham, MA). The capillary voltage was set at 5.5 kV in positive ion mode with a declustering potential of 80V. The mass spectrometer was scanned from 50 to 1000 m/z in operating mode with a 250 ms scan from 50 to 1000 m/z. Melting points were determined on a Fischer-Johns melting point apparatus and are uncorrected. The purity of the compound was established by HPLC using an HP-Agilent 1200 HPLC system on a C18 column, and all the compounds had a purity of >98% unless mentioned.

4.1.2. General procedure for the synthesis of compounds **2(a-l)**

Initially, mono (5 or 7) or di-substituted (5,7) or unsubstituted isatins **1(a-l)** (10 mmol) were dissolved in anhydrous DMF (30 mL) and cooled on ice with stirring. Solid dry K₂CO₃ (11 mmol) was added in one portion, and the dark-colored suspension was brought to room temperature and stirred for a further 1 h. 1,4-bis(bromomethyl)benzene (40 mmol) was added slowly with constant stirring until the mono or di-substituted isatin starting material had been consumed (TLC). The reaction mixture was poured into cold water and extracted with ethyl acetate. The ethyl acetate layer was washed with water, brine, and dried over MgSO₄. The solvent was removed, and the crude product was purified by silica gel column chromatography using (hexanes/EtOAc, 80:20) as eluent to yield the key intermediates (-N-(p-bromomethyl benzyl)isatins **2(a-l)** (yield 75-80%) as orange-red crystals.

4.1.3. General procedure for the synthesis of compounds **3(a-l)**

To each unsubstituted, mono, and di-substituted (-N-(p-bromomethyl benzyl)isatins **2(a-l)** (1.02mmol), thiourea (1.02 mmol) and ethanol (25 ml) was added and heated to reflux until the starting material had been disappeared (TLC). The solvent was removed under vacuum. The crude product was washed with ethyl acetate to remove unreacted (-N-(p-bromomethyl benzyl)isatins. The products **3(a-l)** were recrystallized by ethanol-ethyl acetate with good yields.

4.1.4. General procedure for the synthesis of compounds **4(a-l)**

To each unsubstituted, mono, and di-substituted (*N*-(*p*-bromomethyl benzyl)isatins **2(a-l)** (1.02mmol), selenourea (1.02 mmol) and ethanol (25 ml) was added and heated to reflux until the starting material had been disappeared (TLC). The solvent was removed under vacuum. The crude product was washed with ethyl acetate to remove unreacted (*N*-(*p*-bromomethyl benzyl)isatins. The products **4(a-l)** were recrystallized by ethanol-ethyl acetate with good yields.

4.1.5. 2-[4-(2,3-Dioxo-2,3-dihydroindol-1-ylmethyl)benzyl]isothioureia hydrobromide (**3a**) (**KS104**).

Yellow solid, Yield: 83%; mp: 208-210 °C; ¹H NMR (500 MHz, DMSO-*d*₆): δ 9.18 (s, 2H), 8.98 (s, 2H), 7.61 - 7.57 (m, 2H), 7.46 - 7.38 (m, 4H), 7.13 (dt, *J*=0.6, 7.5 Hz, 1H), 6.98 (dd, *J*=0.5, 8.2 Hz, 1H), 4.92 (s, 2H), 4.47 (s, 2H). ¹³C NMR (150 MHz, DMSO-*d*₆): δ 183.5, 169.5, 158.8, 150.8, 138.5, 135.9, 134.8, 129.8, 128.3, 125.0, 123.9, 118.3, 111.5, 43.1, 34.4. MS (ESI) *m/z* 326 [M+H]; HRMS (ESI) *m/z* for C₁₇H₁₅N₃O₂S calculated 326.0885, found *m/z*: 326.0963.

4.1.6. 2-[4-(5-Bromo-2,3-dioxo-2,3-dihydroindol-1-ylmethyl)benzyl]isothioureia hydrobromide (**3b**) (**KS108**).

Orange solid, Yield: 75%; mp: 217-219 °C; ¹H NMR (500 MHz, DMSO-*d*₆): δ 9.15 - 8.96 (m, 4H), 7.78 - 7.75 (m, 2H), 7.46 - 7.37 (m, 4H), 6.93 (dd, *J*=0.5, 8.2 Hz, 1H), 4.91 (s, 2H), 4.46 (s, 2H). ¹³C NMR (150 MHz, DMSO-*d*₆): δ 182.3, 169.5, 158.5, 149.6, 140.1, 135.6, 134.8, 129.7, 128.2, 127.2, 120.1, 115.6, 113.6, 43.1, 34.4. MS (ESI) *m/z* 404 [M+H]; HR-MS (ESI) *m/z* for C₁₇H₁₄BrN₃O₂S calculated 403.9990, found *m/z*: 404.0075.

4.1.7. 2-[4-(7-Bromo-2,3-dioxo-2,3-dihydroindol-1-ylmethyl)benzyl]isothioureia hydrobromide (**3c**) (**KS110**).

Yellow solid, Yield: 78%; mp: 206-208 °C; ¹H NMR (500 MHz, DMSO-*d*₆): δ 9.18 (s, 2H), 8.99 (s, 2H), 7.76 (dd, *J*=1.2, 8.1 Hz, 1H), 7.65 (dd, *J*=1.2, 7.3 Hz, 1H), 7.39 (m, 4H), 7.10 (dd, *J*=7.4, 8.1 Hz, 1H), 5.26 (s, 2H), 4.48 (s, 2H). ¹³C NMR (150 MHz, DMSO-*d*₆): δ 182.3, 169.5, 159.9, 147.5, 143.3, 137.5, 134.1, 129.6, 127.2, 125.6, 124.5, 122.1, 103.6, 44.4, 34.5. MS (ESI) *m/z* 404 [M+H]; HRMS (ESI) *m/z* for C₁₇H₁₄BrN₃O₂S calculated 403.9990, found *m/z*: 404.0091.

4.1.8. 2-[4-(5-Chloro-2,3-dioxo-2,3-dihydroindol-1-ylmethyl)benzyl]isothioureia hydrobromide (**3d**) (**KS112**).

Orange solid, Yield: 77%; mp: 226-228 °C; ^1H NMR (500 MHz, DMSO- d_6): δ 9.17 (s, 2H), 8.97 (s, 2H), 7.65 - 7.63 (m, 2H), 7.42 (dd, $J=8.2, 26.3$ Hz, 4H), 6.99 (dd, $J=1.6, 7.4$ Hz, 1H), 4.92 (s, 2H), 4.48 (s, 2H). ^{13}C NMR (150 MHz, DMSO- d_6): δ 182.4, 169.5, 158.6, 149.2, 137.3, 135.6, 134.8, 129.7, 128.3, 128.1, 124.5, 119.7, 113.2, 43.2, 34.4. MS (ESI) m/z 360 [M+H]; HRMS (ESI) m/z for $\text{C}_{17}\text{H}_{14}\text{ClN}_3\text{O}_2\text{S}$ calculated 360.0495, found m/z : 360.0570.

4.1.9. 2-[4-(7-Chloro-2,3-dioxo-2,3-dihydroindol-1-ylmethyl)benzyl]isothiourea hydrobromide (3e) (KS114).

Orange solid, Yield: 73%; mp: 225-227 °C; ^1H NMR (600 MHz, DMSO- d_6): δ 9.18 (s, 2H), 9.03 (s, 2H), 7.62 (d, $J=2.4$ Hz, 1H), 7.61 (dd, $J=1.1, 4.4$ Hz, 1H), 7.40 (m, 4H), 7.17 (t, $J=7.7$ Hz, 1H), 5.22 (s, 2H), 4.51 (s, 2H). ^{13}C NMR (150 MHz, DMSO- d_6): δ 182.3, 169.5, 159.8, 146.0, 139.9, 137.5, 134.2, 129.6, 127.2, 125.3, 124.1, 121.8, 116.2, 44.8, 34.5. MS (ESI) m/z 360 [M+H]; HRMS (ESI) m/z for $\text{C}_{17}\text{H}_{14}\text{ClN}_3\text{O}_2\text{S}$ calculated 360.0495, found m/z : 360.0584.

4.1.10. 2-[4-(5-Fluoro-2,3-dioxo-2,3-dihydroindol-1-ylmethyl)benzyl]isothiourea hydrobromide (3f) (KS116).

Orange solid, Yield: 75%; mp: 208-210 °C; ^1H NMR (600 MHz, DMSO- d_6): δ 9.17 (s, 2H), 9.03 (s, 2H), 7.50 (dd, $J=2.4, 7.0$ Hz, 1H), 7.47 (d, $J=8.3$ Hz, 1H), 7.46 (d, $J=8.3$ Hz, 2H), 7.41 (d, $J=8.4$ Hz, 2H), 7.00 (dd, $J=3.8, 8.6$ Hz, 1H), 4.92 (s, 2H), 4.51 (s, 2H). ^{13}C NMR (150 MHz, DMSO- d_6): δ 182.9, 169.5, 159.0, 158.9, 147.0, 135.7, 134.8, 129.8, 128.3, 124.3, 119.2, 112.9, 112.0, 43.2, 34.4. MS (ESI) m/z 344 [M+H]; HRMS (ESI) m/z for $\text{C}_{17}\text{H}_{14}\text{FN}_3\text{O}_2\text{S}$ calculated 344.0791, found m/z : 344.0883.

4.1.11. 2-[4-(7-Fluoro-2,3-dioxo-2,3-dihydroindol-1-ylmethyl)benzyl]isothiourea hydrobromide (3g) (KS118).

Orange solid, Yield: 71%; mp: 210-212 °C; ^1H NMR (600 MHz, DMSO- d_6): δ 9.20 (s, 2H), 9.06 (s, 2H), 7.52 (dd, $J=8.6, 11.6$ Hz, 1H), 7.48 (d, $J=7.3$ Hz, 1H), 7.41 (m, 4H), 7.16 (ddd, $J=7.9, 7.9, 3.8$ Hz, 1H), 4.97 (s, 2H), 4.51 (s, 2H). ^{13}C NMR (150 MHz, DMSO- d_6): δ 182.3, 169.5, 158.9, 147.7, 136.8, 136.5, 134.6, 129.7, 127.7, 126.2, 125.1, 121.5, 121.3, 45.3, 34.4. MS (ESI) m/z 344 [M+H]; HRMS (ESI) m/z for $\text{C}_{17}\text{H}_{14}\text{FN}_3\text{O}_2\text{S}$ calculated 344.0791, found m/z : 344.0882.

4.1.12. 2-[4-(2,3-Dioxo-5-trifluoromethyl-2,3-dihydroindol-1-ylmethyl)benzyl]isothioureahydrobromide (3h) (KS106).

Yellow solid, Yield: 76%; mp: 225-227 °C; ¹H NMR (500 MHz, DMSO-d₆): ¹H NMR (500 MHz, DMSO) δ 9.17 (s, 2H), 9.00 (s, 2H), 7.96 (dd, J=1.3, 8.4 Hz, 1H), 7.89 (d, J=1.7 Hz, 1H), 7.49 - 7.39 (m, 4H), 7.15 (d, J=8.4 Hz, 1H), 4.98 (s, 2H), 4.48 (s, 2H). ¹³C NMR (150 MHz, DMSO-d₆): δ 182.0, 169.5, 159.0, 153.4, 135.5, 134.9, 134.9, 129.7, 128.3, 124.4, 124.2, 121.5, 118.9, 112.0, 43.3, 34.4. MS (ESI) m/z 394 [M+H]; HRMS (ESI) m/z for C₁₈H₁₄F₃N₃O₂S calculated 394.0759, found m/z: 394.0838.

4.1.13. 2-[4-(2,3-Dioxo-7-trifluoromethyl-2,3-dihydroindol-1-ylmethyl)benzyl]isothioureahydrobromide (3i) (KS122).

Yellow solid, Yield: 70%; mp: 216-218 °C; ¹H NMR (600 MHz, DMSO-d₆): ¹H NMR (600 MHz, DMSO) δ 9.23 (s, 2H), 9.05 (s, 2H), 7.95 (d, J=7.6 Hz, 1H), 7.94 (dd, J=1.4, 7.2 Hz, 1H), 7.39 - 7.33 (m, 5H), 5.03 (s, 2H), 4.49 (s, 2H). ¹³C NMR (150 MHz, DMSO-d₆): δ 181.4, 169.5, 160.5, 148.4, 136.5, 135.0, 133.8, 129.4, 129.0, 126.5, 123.9, 123.3, 121.7, 112.8, 46.3, 34.4. MS (ESI) m/z 394 [M+H]; HRMS (ESI) m/z for C₁₈H₁₄F₃N₃O₂S calculated 394.0759, found m/z: 394.0852.

4.1.14. 2-[4-(5, 7-Dibromo-2, 3-dioxo-2, 3-dihydroindol-1-ylmethyl)benzyl]isothioureahydrobromide (3j) (KS100).

Orange solid, Yield: 84%; mp: 196-198 °C; ¹H NMR (500 MHz, DMSO-d₆): δ 9.17 (s, 2H), 8.98 (s, 2H), 8.01 (d, J=2.0 Hz, 1H), 7.82 (d, J=2.0 Hz, 1H), 7.42 - 7.36 (m, 4H), 5.25 (s, 2H), 4.47 (s, 2H). ¹³C NMR (150 MHz, DMSO-d₆): δ 181.1, 169.48, 159.6, 146.7, 143.8, 137.4, 134.1, 129.6, 127.2, 126.8, 123.3, 116.2, 104.7, 44.5, 34.5; MS (ESI) m/z 481 [M+H]; HRMS (ESI) m/z for C₁₇H₁₃Br₂N₃O₂S calculated 481.9173, found m/z: 481.9164.

4.1.15. 2-[4-(5,7-Dichloro-2,3-dioxo-2,3-dihydroindol-1-ylmethyl)benzyl]isothioureahydrobromide (3k) (KS102).

Orange solid, Yield: 81%; mp: 203-205 °C; ¹H NMR (500 MHz, DMSO-d₆): δ 9.22 (s, 2H), 9.04 (s, 2H), 7.78 (d, J=2.1 Hz, 1H), 7.70 (d, J=2.1 Hz, 1H), 7.43 - 7.37 (m, 4H), 5.19 (s, 2H), 4.49 (s, 2H). ¹³C NMR (125 MHz, DMSO-d₆): δ 181.1, 169.5, 159.6, 144.8, 138.0, 137.4, 134.2, 129.6, 128.5,

127.1, 123.7, 122.7, 117.0, 44.8, 34.4. MS (ESI) m/z 394 [M+H]; HRMS (ESI) m/z for $C_{17}H_{13}Cl_2N_3O_2S$ calculated 394.0106, found m/z : 394.0187.

4.1.16. 2-[4-(7-Bromo-5-fluoro-2,3-dioxo-2,3-dihydroindol-1-ylmethyl)benzyl]isothiourea hydrobromide (3I) (KS120).

Orange solid, Yield: 67%; mp: 216-218 °C; 1H NMR (500 MHz, DMSO- d_6): δ 9.25 (s, 2H), 9.14 (s, 2H), 7.79 (dd, $J=2.7, 8.8$ Hz, 1H), 7.63 (dd, $J=2.7, 6.3$ Hz, 1H), 7.37 (m, 4H), 5.23 (s, 2H), 4.50 (s, 2H). ^{13}C NMR (125 MHz, DMSO- d_6): δ 181.6, 166.6, 159.3, 158.7, 144.1, 137.0, 136.1, 129.5, 128.8, 127.1, 122.6, 112.0, 103.5, 44.4, 30.5. MS (ESI) m/z 421 [M+H]; HRMS (ESI) m/z for $C_{17}H_{13}BrFN_3O_2S$ calculated 421.9895, found m/z : 421.9991.

4.1.17. 2-[4-(2,3-Dioxo-2,3-dihydroindol-1-ylmethyl)benzyl]isoselenourea hydrobromide (4a) (KS105).

Yellow solid, Yield: 77%; mp: 216-218 °C; 1H NMR (500 MHz, DMSO- d_6): δ 9.25 (s, 2H), 9.12 (s, 2H), 7.61 - 7.57 (m, 2H), 7.43 - 7.37 (m, 4H), 7.13 (dt, $J=7.5, 7.5, 0.7$ Hz, 1H), 6.99 (dd, $J=0.6, 8.4$ Hz, 1H), 4.90 (s, 2H), 4.50 (s, 2H). ^{13}C NMR (150 MHz, DMSO- d_6): δ 183.5, 166.7, 158.8, 150.8, 138.5, 136.8, 135.5, 129.8, 128.2, 125.0, 123.9, 118.2, 111.5, 43.1, 30.4. MS (ESI) m/z 374 [M+H]; HRMS (ESI) m/z for $C_{17}H_{15}N_3O_2Se$ calculated 374.0329, found m/z : 374.0414.

4.1.18. 2-[4-(5-Bromo-2,3-dioxo-2,3-dihydroindol-1-ylmethyl)benzyl]isoselenourea hydrobromide (4b) (KS109).

Orange solid, Yield: 70%; mp: 208-210 °C; 1H NMR (500 MHz, DMSO- d_6): δ 9.24 (s, 2H), 9.15 (s, 2H), 7.78 - 7.74 (m, 2H), 7.43 - 7.36 (m, 4H), 6.93 (d, $J=8.3$ Hz, 1H), 4.90 (s, 2H), 4.50 (s, 2H). ^{13}C NMR (150 MHz, DMSO- d_6): δ 182.3, 166.7, 158.5, 149.6, 140.1, 136.8, 135.2, 129.7, 128.2, 127.2, 120.1, 115.6, 113.6, 43.2, 30.4. MS (ESI) m/z 451 [M+H]; HRMS (ESI) m/z for $C_{17}H_{14}BrN_3O_2Se$ calculated 451.9435, found m/z : 451.9550.

4.1.19. 2-[4-(7-Bromo-2,3-dioxo-2,3-dihydroindol-1-ylmethyl)benzyl]isoselenourea hydrobromide (4c) (KS111).

Orange solid, Yield: 72%; mp: 202-204 °C; 1H NMR (500 MHz, DMSO- d_6): δ 9.24 (s, 2H), 9.12 (s, 2H), 7.77 (dd, $J=1.2, 8.1$ Hz, 1H), 7.65 (dd, $J=1.2, 7.3$ Hz, 1H), 7.36 (m, 4H), 7.10 (dd, $J=7.3, 8.1$ Hz, 1H), 5.25 (s, 2H), 4.51 (s, 2H). ^{13}C NMR (150 MHz, DMSO): δ 182.3, 166.7, 159.9, 147.5,

143.3, 137.1, 136.1, 129.6, 127.1, 125.6, 124.5, 122.0, 103.6, 44.4, 30.5. . MS (ESI) m/z 451 [M+H]; HRMS (ESI) m/z for $C_{17}H_{14}BrN_3O_2Se$ calculated 451.9435, found m/z : 451.9543.

4.1.20. 2-[4-(5-Chloro-2,3-dioxo-2,3-dihydroindol-1-ylmethyl)benzyl]isoselenourea hydrobromide (4d) (KS113).

Orange solid, Yield: 70%; mp: 216-218 °C; 1H NMR (500 MHz, DMSO- d_6): δ 9.24 (s, 2H), 9.15 (s, 2H), 7.65 - 7.63 (m, 2H), 7.43 - 7.36 (m, 4H), 6.99 (dd, J =1.8, 7.3 Hz, 1H), 4.91 (s, 2H), 4.50 (s, 2H). ^{13}C NMR (150 MHz, DMSO- d_6): δ 182.4, 166.7, 158.6, 149.3, 137.3, 136.9, 135.2, 129.7, 128.2, 128.1, 124.5, 119.7, 113.2, 43.2, 30.4. MS (ESI) m/z 407 [M+H]; HRMS (ESI) m/z for $C_{17}H_{14}ClN_3O_2Se$ calculated 407.9940, found m/z : 408.0035.

4.1.21. 2-[4-(7-Chloro-2,3-dioxo-2,3-dihydroindol-1-ylmethyl)benzyl]isoselenourea hydrobromide (4e) (KS115).

Orange solid, Yield: 70%; mp: 192-194 °C; 1H NMR (500 MHz, DMSO- d_6): δ 9.24 (s, 2H), 9.14 (s, 2H), 7.62 (dd, J =1.2, 7.3 Hz, 1H), 7.61 (dd, J =1.2, 8.2 Hz, 1H), 7.37 (m, 4H), 7.16 (dd, J =7.3, 8.1 Hz, 1H), 5.20 (s, 2H), 4.51 (s, 2H). ^{13}C NMR (150 MHz, DMSO- d_6): δ 182.3, 166.7, 159.8, 146.0, 140.0, 137.1, 136.2, 129.6, 127.1, 125.3, 124.1, 121.8, 116.2, 44.8, 30.5. MS (ESI) m/z 407 [M+H]; HRMS (ESI) m/z for $C_{17}H_{14}ClN_3O_2Se$ calculated 407.9940, found m/z : 408.0041.

4.1.22. 2-[4-(5-Fluoro-2,3-dioxo-2,3-dihydroindol-1-ylmethyl)benzyl]isoselenourea hydrobromide (4f) (KS117).

Orange solid, Yield: 72%; mp: 201-203 °C; 1H NMR (500 MHz, DMSO- d_6): δ 9.25 (s, 2H), 9.12 (s, 2H), 7.52 - 7.44 (m, 2H), 7.43 - 7.37 (m, 4H), 6.98 (dd, J =3.8, 8.6 Hz, 1H), 4.90 (s, 2H), 4.50 (s, 2H). ^{13}C NMR (150 MHz, DMSO- d_6): δ 182.9, 166.7, 159.0, 158.9, 147.0, 136.9, 135.3, 129.8, 128.2, 124.3, 119.2, 112.9, 112.0, 43.2, 30.4. MS (ESI) m/z 392 [M+H]; HRMS (ESI) m/z for $C_{17}H_{14}FN_3O_2Se$ calculated 392.0235, found m/z : 392.0337.

4.1.23. 2-[4-(7-Fluoro-2,3-dioxo-2,3-dihydroindol-1-ylmethyl)benzyl]isoselenourea hydrobromide (4g) (KS119).

Orange solid, Yield: 69%; mp: 206-208 °C; 1H NMR (500 MHz, DMSO- d_6): δ 9.25 (s, 2H), 9.13 (s, 2H), 7.51 (ddd, J =1.0, 8.4, 11.8 Hz, 1H), 7.48 (dd, J =1.0, 7.4 Hz, 1H), 7.38 (m, 4H), 7.15 (ddd, J =4.0, 7.5, 8.3 Hz, 1H), 4.96 (s, 2H), 4.50 (s, 2H). ^{13}C NMR (150 MHz, DMSO- d_6): δ 182.3, 166.7,

158.9, 147.6, 136.6, 136.3, 129.7, 127.6, 126.2, 125.0, 121.4, 121.3, 45.3, 30.5. MS (ESI) m/z 392 [M+H]; HRMS (ESI) m/z for $C_{17}H_{14}FN_3O_2Se$ calculated 392.0235, found m/z : 392.0334.

4.1.24. 2-[4-(2,3-Dioxo-5-trifluoromethyl-2,3-dihydroindol-1-ylmethyl)benzyl]isoselenourea hydrobromide (4h) (KS107).

Yellow solid, Yield: 72%; mp: 218-220 °C; 1H NMR (500 MHz, DMSO- d_6): δ 9.24 (s, 2H), 9.13 (s, 2H), 7.96 (dd, $J=1.2, 8.4$ Hz, 1H), 7.89 (d, $J=1.2$ Hz, 1H), 7.45 - 7.37 (m, 4H), 7.15 (d, $J=8.4$ Hz, 1H), 4.96 (s, 2H), 4.50 (s, 2H). ^{13}C NMR (150 MHz, DMSO): δ 182.1, 166.7, 159.0, 153.4, 136.9, 135.1, 134.9, 129.7, 128.2, 124.4, 124.2, 121.5, 118.9, 112.0, 43.3, 30.4. MS (ESI) m/z 442 [M+H]; HRMS (ESI) m/z for $C_{18}H_{14}F_3N_3O_2Se$ calculated 442.0203, found m/z : 442.0285.

4.1.25. 2-[4-(2,3-Dioxo-7-trifluoromethyl-2,3-dihydroindol-1-ylmethyl)benzyl]isoselenourea hydrobromide (4i) (KS123).

Yellow solid, Yield: 62%; mp: 212-214 °C; 1H NMR (600 MHz, DMSO- d_6): δ 9.25 (s, 2H), 9.13 (s, 2H), 7.85 (d, $J=7.4$ Hz, 1H), 7.75 (d, $J=7.7$ Hz, 1H), 7.36 - 7.31 (m, 5H), 5.05 (s, 2H), 4.50 (s, 2H). ^{13}C NMR (150 MHz, DMSO- d_6): δ 181.3, 166.5, 160.4, 158.4, 136.5, 135.0, 133.6, 129.4, 129.1, 126.5, 123.8, 123.3, 121.8, 112.8, 46.2, 30.4. MS (ESI) m/z 442 [M+H]; HRMS (ESI) m/z for $C_{18}H_{14}F_3N_3O_2Se$ calculated 442.0203, found m/z : 442.0311.

4.1.26. 2-[4-(5, 7-Dibromo-2, 3-dioxo-2, 3-dihydroindol-1-ylmethyl)benzyl]isoselenourea hydrobromide (4j) (KS101).

Orange solid, Yield: 78%; mp: 193-195 °C; 1H NMR (600 MHz, DMSO- d_6): δ 9.29 (s, 2H), 9.17 (s, 2H), 8.01 (d, $J=2.0$ Hz, 1H), 7.81 (d, $J=2.0$ Hz, 1H), 7.38 (m, 4H), 5.24 (s, 2H), 4.54 (s, 2H). ^{13}C NMR (150 MHz, DMSO- d_6): δ 181.1, 166.7, 159.6, 146.7, 143.8, 136.9, 136.1, 129.6, 127.1, 126.8, 123.2, 116.2, 104.7, 44.5, 30.5. MS (ESI) m/z 529 [M+H]; HRMS (ESI) m/z for $C_{17}H_{13}Br_2N_3O_2Se$ calculated 529.8617, found m/z : 529.8618.

4.1.27. 2-[4-(5, 7-Dichloro-2, 3-dioxo-2, 3-dihydroindol-1-ylmethyl)benzyl]isoselenourea hydrobromide (4k) (KS103).

Orange solid, Yield: 76%; mp: 213-215 °C; 1H NMR (500 MHz, DMSO- d_6): δ 9.26 (s, 2H), 9.15 (s, 2H), 8.01 (s, 1H), 7.81 (d, $J=2.0$ Hz, 1H), 7.37 (s, 4H), 5.24 (s, 2H), 4.51 (s, 2H). ^{13}C NMR (150 MHz, DMSO- d_6): δ 181.1, 166.7, 159.6, 146.7, 143.8, 136.9, 136.1, 129.5, 127.1, 126.8, 123.2,

116.2, 104.7, 44.5, 30.5. MS (ESI) m/z 441 [M+H]; HR-MS (ESI) m/z for $C_{17}H_{13}Cl_2N_3O_2Se$ calculated 441.9550, found m/z : 441.9545.

4.1.28. 2-[4-(7-Bromo-5-fluoro-2,3-dioxo-2,3-dihydroindol-1-ylmethyl)benzyl]isoselenourea hydrobromide (**4I**) (**KS121**).

Orange solid, Yield: 65%; mp: 195-197 °C; 1H NMR (600 MHz, DMSO- d_6): δ 9.23 (s, 2H), 9.12 (s, 2H), 7.79 (dd, $J=2.7, 8.7$ Hz, 1H), 7.63 (dd, $J=2.6, 6.2$ Hz, 1H), 7.37 (m, 4H), 5.24 (s, 2H), 4.51 (s, 2H). ^{13}C NMR (150 MHz, DMSO- d_6): δ 181.6, 166.6, 159.2, 158.8, 144.1, 137.0, 136.1, 129.5, 128.9, 127.1, 122.6, 112.0, 103.6, 44.4, 30.5. MS (ESI) m/z 469 [M+H]; HRMS (ESI) m/z for $C_{17}H_{13}BrFN_3O_2Se$ calculated 469.9340, found m/z : 469.9437.

4.2. Biology

4.2.1. Cell line and culture conditions

Dr. Craig Myers, Penn State College of Medicine, Hershey, PA, provided normal human fibroblasts (FF2441). The mutant V600E-BRAF human melanoma cell line 1205 Lu was provided by Dr. Herlyn; Wistar Institute, Philadelphia, PA, and UACC 903 was provided by Dr. Mark Nelson; University of Arizona, Tucson, AZ. Colon cancer cells (HCT116, HT29) and multiple myeloma cells (NCIH929, U266, RPMI8226, MM.1R, MM.1S) were procured from ATCC. Cell lines were maintained in a 37°C humidified 5% CO₂ atmosphere incubator and periodically monitored for phenotypic, genotypic characteristics, and tumorigenic potential to validate and confirm cell line identity.

4.2.2. Molecular docking studies

Binding interactions of isatin and isatin derivatives with ALDH1A1 (PDB: 4X4L), ALDH2 (PDB: 5L13), and ALDH3A1 (PDB: 4L2O) proteins were analyzed using the GLIDE (Grid Ligand Docking with Energetics) docking application in Maestro 10.1 software as described previously [56-58]. Proteins were prepared using the protein preparation wizard tool (Schrodinger, LLC, 2017) with default parameters. The proteins were optimized and minimized for spatial conformations. Grids were generated based on the location of the crystal ligand-binding site (CM037 for ALDH1A1, psoralen for ALDH2, and CB7 for ALDH3A1), using the GLIDE grid module. Default parameters were used, and no constraints were included during grid generation. Ligand preparation was then

performed using the ligprep module in Schrodinger as previously described [56-58]. The docking study was performed using GLIDE 6.6 in Maestro 10.1. The GLIDE algorithm estimates a systematic search of positions, orientations, and conformations of the ligand in the enzyme-binding pocket via a series of hierarchical filters. All hits were subjected to the extra precision (XP) mode of GLIDE. During the docking process, the GLIDE score was used to select the best conformation for each ligand [56-58].

4.2.3. Predicted drug-like properties of compounds.

Drug-like properties of the designed compounds were predicted by using the Quikprops module of Maestro 10.1 software [56-58].

4.2.4. ALDH isoform-specific enzyme assays

ALDH1A1, ALDH2, and ALDH3A1 enzyme assays were performed as described by the manufacturer (R & D systems). Isoform-specific aldehydes were converted to their respective carboxylic acids along with the conversion of NAD⁺ to NADH (absorbance at 340 nm). Specifically, 1 µg/mL of ALDH1A1 was treated with different concentrations of **3(a-l)** and **4(a-l)** for 15 minutes followed by addition of substrate mixture (10 mM propionaldehyde; 100 mM KCl; 1 mM NAD; 2 mM DTT; 50 mM Tris pH 8.5) and the absorbance of NADH was measured in kinetic mode for 5 minutes. Similarly, 0.5 µg/mL of ALDH2 was used in the reaction with 2 mM of acetaldehyde as the substrate, and 0.2 µg/mL of ALDH3A1 was used in the reaction with 1 mM of 4-nitrobenzaldehyde as the substrate.

4.2.5. Cell viability assay

Melanoma, colon cancer, multiple myeloma, and FF2441 cells treated with **3a** or **3(h-l)** and cell viability assays were performed as described previously [54, 59, 60]. Briefly, 5,000 cells per well were plated in a 96-well plate and incubated overnight at 37°C in a 5% CO₂ atmosphere. Cells were treated with **3a** or **3(h-l)** at various concentrations and incubated for 72 hours. Additionally, cells were also treated with 10 mM of NAC. 20 µL of MTS reagent was then added into each well, and the formation of tetrazolium was measured by absorbance after 1 hour at 492 nm. IC₅₀ values for each experimental group were measured in 3 independent experiments using GraphPad Prism version 7.04 (GraphPad Software, La Jolla, CA). Selectivity indices for **3(h-l)** were calculated as a ratio of IC₅₀s in fibroblasts/average of IC₅₀s in melanoma cell lines.

4.2.6. Toxicity studies

To determine the toxicity of **3(h-l)**, compounds (5 mg/kg/day) were injected i.p. into Swiss-Webster mice once daily for 14 days [61, 62]. Animals were monitored for changes in body weight, behavior, and physical distress compared to DMSO control.

4.2.7. ROS assay

ROS activity was measured using DCFDA dye [54]. Briefly, cells were treated with 5 μ M of **3a**, **3h**, or **3j** for 24 hours. Additionally, cells were also treated with 10 mM of NAC. Cells were incubated with 10 μ M of DCFDA for 1 hour, and fluorescence was measured at 485 nm excitation and 510 nm emission. ROS levels in treated cells were compared to DMSO control.

4.2.8. Lipid peroxidation and toxic aldehyde accumulation

Lipid peroxidation and toxic aldehyde accumulation were measured using the thiobarbituric acid reactive substances (TBARS) kit according to the manufacturer's instructions [55]. Briefly, cells were treated with 5 μ M of **3a**, **3h**, or **3j** for 24 hours. Additionally, cells were also treated with 10 mM of NAC. Cell pellets were lysed in PBS by sonication on ice. Lipids in the lysates were hydrolyzed in the presence of acetic acid and sodium hydroxide. Free MDA released from lipids was measured by the reaction to TBA colorimetrically at 530 nm. Lipid peroxidation in treated cells was compared to DMSO control.

4.2.9. Apoptosis assay

Apoptosis assay was measured using Annexin-V-PE/7-AAD kit according to the manufacturer's instructions [54]. Briefly, cells were treated with 5 μ M of **3a**, **3h**, or **3j** for 24 hours. Additionally, cells were also treated with 10 mM of NAC. Cells were detached, washed with PBS, and stained with Annexin-V-PE and 7-AAD. Cells were acquired by BD Fortessa flow cytometer from Penn State Hershey Flow Cytometry core facility. Cells that are double-positive for both Annexin-V and 7-AAD were considered late-stage apoptotic and are compared to DMSO control.

4.2.10. Cell cycle analysis

Cell cycle analysis was performed using Propidium iodide staining [54]. Briefly, cells were treated with 5 μ M of **3a**, **3h**, or **3j** for 24 hours. Additionally, cells were also treated with 10 mM of NAC. Cells were detached, washed with PBS, and fixed in 70% ethanol solution. Cells were stained with

Propidium iodide and acquired by BD Fortessa flow cytometer from Penn State Hershey Flow Cytometry core facility. Cell cycle analysis was performed using FlowJo software.

4.2.11. Statistics

Statistical analysis was undertaken using the one-way/two-way ANOVA GraphPad PRISM Version 7.04 software. Dunnett's as post hoc analysis was performed when there was a significant difference. A p-value of <0.05 was considered statistically significant.

Acknowledgements

Authors thank the co-operation of the Penn State Cancer Institute, Organic Synthesis Core, Flow Cytometry Core, NMR facility in Penn State College of Medicine, Hershey, PA. Authors also thank the assistance of Mass Spectroscopy Core in Huck Institutes of the Life Sciences, Penn State University, University Park, PA.

Schemes:

Scheme 1. Synthesis of compounds **3(a-l)** and **4(a-l)**. Reagents and conditions: a) K_2CO_3 , DMF, 1,4-bis(bromomethyl)benzene; b) Thiourea, EtOH, 90°C; c) Selenourea, EtOH, 90°C.

Figure legends:

Figure 1. Isatin based structures ALDH1A1, ALDH2, and ALDH3A1 inhibitors.

Figure 2. Molecular docking studies of compounds in the active site pockets of ALDH1A1, ALDH2, and ALDH3A1. **3h** is shown as a representative compound for **3(a-l)** and **4(a-l)**.

Figure 3. ROS and lipid peroxidation activity and toxic aldehyde accumulation. HCT116 (**A**) and SW480 (**B**) cells were treated with 5 μ M of **3a**, **3h**, or **3j** for 24 hours with or without NAC (10 mM). ROS levels were measured using DCFDA dye and compared to DMSO control. Malondialdehyde (MDA) levels were measured in colon cancer cell line HCT116 using thiobarbituric acid and compared to DMSO control (**C**). Cell survival assay was performed by MTS assay (**D**), apoptosis by Annexin-V/7-AAD (**E**) and cell cycle by propidium iodide staining in colon cancer cell line HCT116 (**F**).

Table legends:

Table 1. Structures and docking scores of **3(a-l)** and **4(a-l)**. Docking scores were calculated for compounds against ALDH1A1, ALDH2, and ALDH3A1 using the Glide module of Schrodinger.

Table 2. ALDH enzyme inhibitory IC₅₀s of **3(a-l)** and **4(a-l)**. Compounds **3(a-l)** and **4(a-l)** were evaluated for ALDH1A1, ALDH2, and ALDH3A1 inhibitory activity. The % inhibition was calculated for each compound and compared to DMSO control.

Table 3. *in vitro* anti-proliferative activity of selected compounds **3(h-l)**. Compounds **3(h-l)** were evaluated for anti-proliferative effects on melanoma, colon cancer, multiple myeloma, and normal human fibroblasts (FF2441). Cells were treated with **3(h-l)** at various concentrations for 72 hours, and IC₅₀s were calculated.

^a IC₅₀ = Compound concentration required to inhibit cell proliferation by 50%. Data are expressed as the mean \pm SD from the dose-response curve of at least three independent experiments. ND-not determined.

^b Melanoma

^c Colon cancer

^d Multiple myeloma

^e Normal human fibroblasts

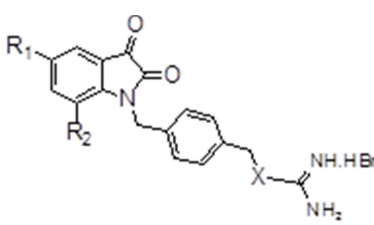
Table 4. Drug-like properties of 3(h-l). Drug-like properties of **3(h-l)** were predicted by Quikprops module of Schrodinger.

SASA: solvent accessible surface area; donor HB: Estimated number of hydrogen bonds that would be donated by the solute to water molecules in an aqueous solution; aacptHB: Estimated number of hydrogen bonds that would be accepted by the solute from water molecules in an aqueous solution; QPlogPo/w: Predicted octanol/water partition coefficient; QPlogHERG: Predicted IC₅₀ value for blockage of HERG K⁺ channels; QPPCaco: Predicted apparent Caco-2 cell permeability in nm/sec. Caco2 cells are a model for the gut-blood barrier; QPlogBB: Predicted brain/blood partition coefficient; QPPMDCK: Predicted apparent MDCK cell permeability in nm/sec; #metab: Number of likely metabolic reactions; Human Oral Absorption: Predicted qualitative human oral absorption; Percent Human Oral Absorption: Predicted human oral absorption on 0 to 100% scale; Rule Of Five: Number of violations of Lipinski's rule of five.

Table 5. Toxicity of 3(h-l). Compounds **3(h-l)** were dosed daily at 5 mg/kg/day via i.p. injection to Swiss-Webster mice for 14 days. % change in animal weight was compared to DMSO control.

Journal Pre-proof

Table 1.



Compound	#	R ₁	R ₂	X	Docking scores		
					ALDH1A1	ALDH2	ALDH3A1
KS104	3a	H	H	S	-10.71	-8.51	-13.383
KS108	3b	Br	H	S	-11.637	-10.28	-13.369
KS110	3c	H	Br	S	-9.727	-7.308	-13.358
KS112	3d	Cl	H	S	-11.938	-11.024	-13.666
KS114	3e	H	Cl	S	-11.271	-7.061	-14.237
KS116	3f	F	H	S	-11.056	-11.03	-12.157
KS118	3g	H	F	S	-11.197	-11.205	-14.24
KS106	3h	CF ₃	H	S	-11.721	-10.374	-12.229
KS122	3i	H	CF ₃	S	-10.836	-9.497	-14.564
KS100	3j	Br	Br	S	-10.247	-8.716	-13.851
KS102	3k	Cl	Cl	S	-10.841	-8.169	-14.103
KS120	3l	F	Br	S	-10.432	-7.294	-13.039
KS105	4a	H	H	Se	-11.487	-10.592	-12.375
KS109	4b	Br	H	Se	-10.149	-6.82	-14.441
KS111	4c	H	Br	Se	-10.144	-6.804	-14.507
KS113	4d	Cl	H	Se	-10.14	-6.756	-13.268
KS115	4e	H	Cl	Se	-10.841	-6.978	-13.85
KS117	4f	F	H	Se	-10.144	-7.929	-12.119
KS119	4g	H	F	Se	-8.387	-8.609	-13.943
KS107	4h	CF ₃	H	Se	-9.988	-11.146	-14.229
KS123	4i	H	CF ₃	Se	-11.741	-9.494	-13.46
KS101	4j	Br	Br	Se	-10.149	-8.975	-12.638
KS103	4k	Cl	Cl	Se	-10.594	-10.841	-13.701
KS121	4l	F	Br	Se	-7.495	-9.792	-12.567

Table 2.

Enzyme inhibition - IC ₅₀ (nM)			
Compound	ALDH1A1	ALDH2	ALDH3A1
3a	4633	>10000	4205
3b	8524	>10000	4878
3c	1713	>10000	6323
3d	>10000	>10000	3067
3e	177	>10000	3586
3f	5224	>10000	2855
3g	598	>10000	241
3h	334	2137	360
3i	268	1783	246
3j	230	1542	193
3k	279	1642	219
3l	285	1782	219
4a	>10000	>10000	4007
4b	333	939	344
4c	360	>10000	>10000
4d	>10000	>10000	2767
4e	>10000	>10000	>10000
4f	5192	>10000	2364
4g	1054	>10000	246
4h	6492	>10000	1520
4i	657	3491	251
4j	397	2012	333
4k	384	1809	327
4l	420	1917	368

Table 3.

[illegible]

Table 4.

Compd	SASA	Donor HB	Accpt HB	QPlogPo/w	QPlogHERG	QPPCaco	QPlogBB	QPPMDCK	#metab	Human Oral Absorption	Percent Human Oral Absorption	Rule of five
3j	645.543	3	6.5	2.69	-5.67	88.143	-1.6	297.149	2	3	77.508	0
3k	636.119	3	6.5	2.545	-5.614	87.592	-1.612	255.413	2	3	76.616	0
3h	638.908	3	6.5	2.503	-5.499	71.546	-1.712	187.952	2	3	74.796	0
3l	467.728	0	5	1.683	-5.005	1064.261	-0.432	529.159	1	3	90.976	0
3i	572.826	0	5	3.86	-5.178	1304.932	0.179	10000	1	3	100	0

Table 5.

Compound	Day 1	Day 7	Day 14	% of weight loss compared to control (at day 14)	P-value compared to DMSO
DMSO	22.9	24.2	24.4	-	-
3h	22.5	20.6	23.8	2%	0.6006
3i	23.1	20.7	20.9	11%	<0.0001
3j	22.7	18.7	19.4	12%	<0.0001
3k	22.4	19.6	20.3	10%	<0.0001
3l	22.6	20.9	20.2	15%	<0.0001

References

- [1] B. Jackson, C. Brocker, D.C. Thompson, W. Black, K. Vasiliou, D.W. Nebert, V. Vasiliou, Update on the aldehyde dehydrogenase gene (ALDH) superfamily, *Hum Genomics*, 5 (2011) 283-303.
- [2] R. Januchowski, K. Wojtowicz, M. Zabel, The role of aldehyde dehydrogenase (ALDH) in cancer drug resistance, *Biomed Pharmacother*, 67 (2013) 669-680.
- [3] J.S. Rodriguez-Zavala, L.F. Calleja, R. Moreno-Sanchez, B. Yoval-Sanchez, Role of Aldehyde Dehydrogenases in Physiopathological Processes, *Chem Res Toxicol*, (2019).
- [4] T. Grune, Protein Oxidation Products as Biomarkers, *Free Radic Biol Med*, 75 Suppl 1 (2014) S7.
- [5] M. Shoeb, N.H. Ansari, S.K. Srivastava, K.V. Ramana, 4-Hydroxynonenal in the pathogenesis and progression of human diseases, *Curr Med Chem*, 21 (2014) 230-237.
- [6] S.E. Allison, Y. Chen, N. Petrovic, J. Zhang, K. Bourget, P.I. Mackenzie, M. Murray, Activation of ALDH1A1 in MDA-MB-468 breast cancer cells that over-express CYP2J2 protects against paclitaxel-dependent cell death mediated by reactive oxygen species, *Biochem Pharmacol*, 143 (2017) 79-89.
- [7] J.A. Ajani, X. Wang, S. Song, A. Suzuki, T. Taketa, K. Sudo, R. Wadhwa, W.L. Hofstetter, R. Komaki, D.M. Maru, J.H. Lee, M.S. Bhutani, B. Weston, V. Baladandayuthapani, Y. Yao, S. Honjo, A.W. Scott, H.D. Skinner, R.L. Johnson, D. Berry, ALDH-1 expression levels predict response or resistance to preoperative chemoradiation in resectable esophageal cancer patients, *Mol Oncol*, 8 (2014) 142-149.
- [8] C.P. Huang, M.F. Tsai, T.H. Chang, W.C. Tang, S.Y. Chen, H.H. Lai, T.Y. Lin, J.C. Yang, P.C. Yang, J.Y. Shih, S.B. Lin, ALDH-positive lung cancer stem cells confer resistance to epidermal growth factor receptor tyrosine kinase inhibitors, *Cancer Lett*, 328 (2013) 144-151.
- [9] E. Charafe-Jauffret, C. Ginestier, F. Iovino, C. Tarpin, M. Diebel, B. Esterni, G. Houvenaeghel, J.M. Extra, F. Bertucci, J. Jacquemier, L. Xerri, G. Dontu, G. Stassi, Y. Xiao, S.H. Barsky, D. Birnbaum, P. Viens, M.S. Wicha, Aldehyde dehydrogenase 1-positive cancer stem cells mediate metastasis and poor clinical outcome in inflammatory breast cancer, *Clin Cancer Res*, 16 (2010) 45-55.
- [10] P. Marcato, C.A. Dean, C.A. Giacomantonio, P.W. Lee, Aldehyde dehydrogenase: its role as a cancer stem cell marker comes down to the specific isoform, *Cell Cycle*, 10 (2011) 1378-1384.
- [11] E. Durinikova, Z. Kozovska, M. Poturnajova, J. Plava, Z. Cierna, A. Babelova, R. Bohovic, S. Schmidtova, M. Tomas, L. Kucerovala, M. Matuskova, ALDH1A3 upregulation and spontaneous metastasis formation is associated with acquired chemoresistance in colorectal cancer cells, *BMC Cancer*, 18 (2018) 848.
- [12] X. Chen, Q. Li, X. Liu, C. Liu, R. Liu, K. Rycaj, D. Zhang, B. Liu, C. Jeter, T. Calhoun-Davis, K. Lin, Y. Lu, H.P. Chao, J. Shen, D.G. Tang, Defining a Population of Stem-like Human Prostate Cancer Cells That Can Generate and Propagate Castration-Resistant Prostate Cancer, *Clin Cancer Res*, 22 (2016) 4505-4516.
- [13] L. Lin, D. Jou, Y. Wang, H. Ma, T. Liu, J. Fuchs, P.K. Li, J. Lu, C. Li, J. Lin, STAT3 as a potential therapeutic target in ALDH+ and CD44+/CD24+ stem cell-like pancreatic cancer cells, *Int J Oncol*, 49 (2016) 2265-2274.
- [14] I. Kurth, L. Hein, K. Mabert, C. Peitzsch, L. Koi, M. Cojoc, L. Kunz-Schughart, M. Baumann, A. Dubrovskaya, Cancer stem cell related markers of radioresistance in head and neck squamous cell carcinoma, *Oncotarget*, 6 (2015) 34494-34509.

- [15] S. Sarvi, R. Crispin, Y. Lu, L. Zeng, T.D. Hurley, D.R. Houston, A. von Kriegsheim, C.H. Chen, D. Mochly-Rosen, M. Ranzani, M.E. Mathers, X. Xu, W. Xu, D.J. Adams, N.O. Carragher, M. Fujita, L. Schuchter, A. Unciti-Broceta, V.G. Brunton, E.E. Patton, ALDH1 Bio-activates Nifuroxazide to Eradicate ALDH(High) Melanoma-Initiating Cells, *Cell Chem Biol*, 25 (2018) 1456-1469 e1456.
- [16] L. Cortes-Dericks, L. Froment, R. Boesch, R.A. Schmid, G. Karoubi, Cisplatin-resistant cells in malignant pleural mesothelioma cell lines show ALDH(high)CD44(+) phenotype and sphere-forming capacity, *BMC Cancer*, 14 (2014) 304.
- [17] M. Flahaut, N. Jauquier, N. Chevalier, K. Nardou, K. Balmas Bourloud, J.M. Joseph, D. Barras, C. Widmann, N. Gross, R. Renella, A. Muhlethaler-Mottet, Aldehyde dehydrogenase activity plays a Key role in the aggressive phenotype of neuroblastoma, *BMC Cancer*, 16 (2016) 781.
- [18] O. Awad, J.T. Yustein, P. Shah, N. Gul, V. Katuri, A. O'Neill, Y. Kong, M.L. Brown, J.A. Toretsky, D.M. Loeb, High ALDH activity identifies chemotherapy-resistant Ewing's sarcoma stem cells that retain sensitivity to EWS-FLI1 inhibition, *PLoS One*, 5 (2010) e13943.
- [19] J.S. Moreb, D. Mohuczy, B. Ostmark, J.R. Zucali, RNAi-mediated knockdown of aldehyde dehydrogenase class-1A1 and class-3A1 is specific and reveals that each contributes equally to the resistance against 4-hydroperoxycyclophosphamide, *Cancer Chemother Pharmacol*, 59 (2007) 127-136.
- [20] G. Muzio, M. Maggiora, E. Paiuzzi, M. Oraldi, R.A. Canuto, Aldehyde dehydrogenases and cell proliferation, *Free Radic Biol Med*, 52 (2012) 735-746.
- [21] E. Vlashi, F. Pajonk, Cancer stem cells, cancer cell plasticity and radiation therapy, *Semin Cancer Biol*, 31 (2015) 28-35.
- [22] C.G. Bazewicz, S.S. Dinavahi, T.D. Schell, G.P. Robertson, Aldehyde Dehydrogenase in Regulatory T Cell Development, *Immunity and Cancer, Immunology*, (2018).
- [23] V. Koppaka, D.C. Thompson, Y. Chen, M. Ellermann, K.C. Nicolaou, R.O. Juvonen, D. Petersen, R.A. Deitrich, T.D. Hurley, V. Vasiliou, Aldehyde dehydrogenase inhibitors: a comprehensive review of the pharmacology, mechanism of action, substrate specificity, and clinical application, *Pharmacol Rev*, 64 (2012) 520-539.
- [24] N. Matsunaga, T. Ogino, Y. Hara, T. Tanaka, S. Koyanagi, S. Ohdo, Optimized Dosing Schedule Based on Circadian Dynamics of Mouse Breast Cancer Stem Cells Improves the Antitumor Effects of Aldehyde Dehydrogenase Inhibitor, *Cancer Res*, 78 (2018) 3698-3708.
- [25] C.A. Morgan, B. Parajuli, C.D. Buchman, K. Dria, T.D. Hurley, N,N-diethylaminobenzaldehyde (DEAB) as a substrate and mechanism-based inhibitor for human ALDH isoenzymes, *Chem Biol Interact*, 234 (2015) 18-28.
- [26] G. Fournet, G. Martin, G. Quash, alpha,beta-Acetylenic Amino Thiolester Inhibitors of Aldehyde Dehydrogenases 1&3: Suppressors of Apoptogenic Aldehyde Oxidation and Activators of Apoptosis, *Current Medicinal Chemistry*, 20 (2013) 527-533.
- [27] M. Perez-Alea, K. McGrail, S. Sanchez-Redondo, B. Ferrer, G. Fournet, J. Cortes, E. Munoz, J. Hernandez-Losa, S. Tenbaum, G. Martin, R. Costello, I. Ceylan, V. Garcia-Patos, J.A. Recio, ALDH1A3 is epigenetically regulated during melanocyte transformation and is a target for melanoma treatment, *Oncogene*, 36 (2017) 5695-5708.
- [28] G. Venton, M. Perez-Alea, C. Baier, G. Fournet, G. Quash, Y. Labiad, G. Martin, F. Sanderson, P. Poullin, P. Suchon, L. Farnault, C. Nguyen, C. Brunet, I. Ceylan, R.T. Costello, Aldehyde dehydrogenases inhibition eradicates leukemia stem cells while sparing normal progenitors, *Blood Cancer J*, 6 (2016) e469.

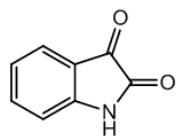
- [29] M.L. Thomas, R. de Antueno, K.M. Coyle, M. Sultan, B.M. Cruickshank, M.A. Giacomantonio, C.A. Giacomantonio, R. Duncan, P. Marcato, Citral reduces breast tumor growth by inhibiting the cancer stem cell marker ALDH1A3, *Mol Oncol*, 10 (2016) 1485-1496.
- [30] S. Zeng, A. Kapur, M.S. Patankar, M.P. Xiong, Formulation, Characterization, and Antitumor Properties of Trans- and Cis-Citral in the 4T1 Breast Cancer Xenograft Mouse Model, *Pharm Res*, 32 (2015) 2548-2558.
- [31] M. Khanna, C.H. Chen, A. Kimble-Hill, B. Parajuli, S. Perez-Miller, S. Baskaran, J. Kim, K. Dria, V. Vasiliou, D. Mochly-Rosen, T.D. Hurley, Discovery of a novel class of covalent inhibitor for aldehyde dehydrogenases, *J Biol Chem*, 286 (2011) 43486-43494.
- [32] J. Kim, J.H. Shin, C.H. Chen, L. Cruz, L. Farnebo, J. Yang, P. Borges, G. Kang, D. Mochly-Rosen, J.B. Sunwoo, Targeting aldehyde dehydrogenase activity in head and neck squamous cell carcinoma with a novel small molecule inhibitor, *Oncotarget*, 8 (2017) 52345-52356.
- [33] S. Okazaki, S. Shintani, Y. Hirata, K. Suina, T. Semba, J. Yamasaki, K. Umene, M. Ishikawa, H. Saya, O. Nagano, Synthetic lethality of the ALDH3A1 inhibitor dyclonine and xCT inhibitors in glutathione deficiency-resistant cancer cells, *Oncotarget*, 9 (2018) 33832-33843.
- [34] A.C. Kimble-Hill, B. Parajuli, C.H. Chen, D. Mochly-Rosen, T.D. Hurley, Development of selective inhibitors for aldehyde dehydrogenases based on substituted indole-2,3-diones, *J Med Chem*, 57 (2014) 714-722.
- [35] C.A. Morgan, T.D. Hurley, Characterization of two distinct structural classes of selective aldehyde dehydrogenase 1A1 inhibitors, *J Med Chem*, 58 (2015) 1964-1975.
- [36] S.M. Yang, A. Yasgar, B. Miller, M. Lal-Nag, K. Brimacombe, X. Hu, H. Sun, A. Wang, X. Xu, K. Nguyen, U. Oppermann, M. Ferrer, V. Vasiliou, A. Simeonov, A. Jadhav, D.J. Maloney, Discovery of NCT-501, a Potent and Selective Theophylline-Based Inhibitor of Aldehyde Dehydrogenase 1A1 (ALDH1A1), *J Med Chem*, 58 (2015) 5967-5978.
- [37] S.M. Yang, N.J. Martinez, A. Yasgar, C. Danchik, C. Johansson, Y. Wang, B. Baljinnyam, A.Q. Wang, X. Xu, P. Shah, D. Cheff, X.S. Wang, J. Roth, M. Lal-Nag, J.E. Dunford, U. Oppermann, V. Vasiliou, A. Simeonov, A. Jadhav, D.J. Maloney, Discovery of Orally Bioavailable, Quinoline-Based Aldehyde Dehydrogenase 1A1 (ALDH1A1) Inhibitors with Potent Cellular Activity, *J Med Chem*, 61 (2018) 4883-4903.
- [38] S. Kulsum, H.V. Sudheendra, R. Pandian, D.R. Ravindra, G. Siddappa, N. R, P. Chevour, B. Ramachandran, M. Sagar, A. Jayaprakash, A. Mehta, V. Kekatpure, N. Hedne, M.A. Kuriakose, A. Suresh, Cancer stem cell mediated acquired chemoresistance in head and neck cancer can be abrogated by aldehyde dehydrogenase 1 A1 inhibition, *Mol Carcinog*, 56 (2017) 694-711.
- [39] B.C. Huddle, E. Grimley, C.D. Buchman, M. Chtcherbinine, B. Debnath, P. Mehta, K. Yang, C.A. Morgan, S. Li, J. Felton, D. Sun, G. Mehta, N. Neamati, R.J. Buckanovich, T.D. Hurley, S.D. Larsen, Structure-Based Optimization of a Novel Class of Aldehyde Dehydrogenase 1A (ALDH1A) Subfamily-Selective Inhibitors as Potential Adjuncts to Ovarian Cancer Chemotherapy, *J Med Chem*, 61 (2018) 8754-8773.
- [40] B. Parajuli, M.L. Fishel, T.D. Hurley, Selective ALDH3A1 inhibition by benzimidazole analogues increase mafosfamide sensitivity in cancer cells, *J Med Chem*, 57 (2014) 449-461.
- [41] S.S. Dinavahi, C.G. Bazewicz, R. Gowda, G.P. Robertson, Aldehyde Dehydrogenase Inhibitors for Cancer Therapeutics, *Trends Pharmacol Sci*, 40 (2019) 774-789.
- [42] G. Krishnegowda, A.S. Prakasha Gowda, H.R. Tagaram, K.F. Carroll, R.B. Irby, A.K. Sharma, S. Amin, Synthesis and biological evaluation of a novel class of isatin analogs as dual inhibitors of tubulin polymerization and Akt pathway, *Bioorg Med Chem*, 19 (2011) 6006-6014.

- [43] M.K. Pandey, K. Gowda, S.S. Sung, T. Abraham, T. Budak-Alpdogan, G. Talamo, S. Dovat, S. Amin, A novel dual inhibitor of microtubule and Bruton's tyrosine kinase inhibits survival of multiple myeloma and osteoclastogenesis, *Experimental hematology*, 53 (2017) 31-42.
- [44] C. Annageldiyev, K. Gowda, T. Patel, P. Bhattacharya, S.F. Tan, S. Iyer, D. Desai, S. Dovat, D.J. Feith, T.P. Loughran, Jr., S. Amin, D. Claxton, A. Sharma, The novel Isatin analog KS99 targets stemness markers in acute myeloid leukemia, *Haematologica*, (2019).
- [45] Y. Luo, K. Dallaglio, Y. Chen, W.A. Robinson, S.E. Robinson, M.D. McCarter, J. Wang, R. Gonzalez, D.C. Thompson, D.A. Norris, D.R. Roop, V. Vasilidou, M. Fujita, ALDH1A isozymes are markers of human melanoma stem cells and potential therapeutic targets, *Stem Cells*, 30 (2012) 2100-2113.
- [46] L. Yue, Z.M. Huang, S. Fong, S. Leong, J.G. Jakowatz, A. Charruyer-Reinwald, M. Wei, R. Ghadially, Targeting ALDH1 to decrease tumorigenicity, growth and metastasis of human melanoma, *Melanoma Res*, 25 (2015) 138-148.
- [47] P. Dalerba, S.J. Dylla, I.K. Park, R. Liu, X. Wang, R.W. Cho, T. Hoey, A. Gurney, E.H. Huang, D.M. Simeone, A.A. Shelton, G. Parmiani, C. Castelli, M.F. Clarke, Phenotypic characterization of human colorectal cancer stem cells, *Proceedings of the National Academy of Sciences of the United States of America*, 104 (2007) 10158-10163.
- [48] A. Lugli, G. Iezzi, I. Hostettler, M.G. Muraro, V. Mele, L. Tornillo, V. Carafa, G. Spagnoli, L. Terracciano, I. Zlobec, Prognostic impact of the expression of putative cancer stem cell markers CD133, CD166, CD44s, EpCAM, and ALDH1 in colorectal cancer, *British journal of cancer*, 103 (2010) 382-390.
- [49] W. Matsui, Q. Wang, J.P. Barber, S. Brennan, B.D. Smith, I. Borrello, I. McNiece, L. Lin, R.F. Ambinder, C. Peacock, D.N. Watkins, C.A. Huff, R.J. Jones, Clonogenic multiple myeloma progenitors, stem cell properties, and drug resistance, *Cancer Res*, 68 (2008) 190-197.
- [50] S. Deng, X. Yang, H. Lassus, S. Liang, S. Kaur, Q. Ye, C. Li, L.P. Wang, K.F. Roby, S. Orsulic, D.C. Connolly, Y. Zhang, K. Montone, R. Butzow, G. Coukos, L. Zhang, Distinct expression levels and patterns of stem cell marker, aldehyde dehydrogenase isoform 1 (ALDH1), in human epithelial cancers, *PLoS One*, 5 (2010) e10277.
- [51] C. Ginestier, M.H. Hur, E. Charafe-Jauffret, F. Monville, J. Dutcher, M. Brown, J. Jacquemier, P. Viens, C.G. Kleer, S. Liu, A. Schott, D. Hayes, D. Birnbaum, M.S. Wicha, G. Dontu, ALDH1 is a marker of normal and malignant human mammary stem cells and a predictor of poor clinical outcome, *Cell Stem Cell*, 1 (2007) 555-567.
- [52] Y. Yang, W. Zhou, J. Xia, Z. Gu, E. Wendlandt, X. Zhan, S. Janz, G. Tricot, F. Zhan, NEK2 mediates ALDH1A1-dependent drug resistance in multiple myeloma, *Oncotarget*, 5 (2014) 11986-11997.
- [53] S.S. Dinavahi, R. Gowda, K. Gowda, C.G. Bazewicz, V.R. Chirasani, M.B. Battu, A. Berg, N.V. Dokholyan, S. Amin, G.P. Robertson, Development of a novel multi-isoform ALDH inhibitor effective as an anti-melanoma agent, *Mol Cancer Ther*, (2019).
- [54] P.C. Rao, S. Begum, M. Sahai, D.S. Sriram, Coptisine-induced cell cycle arrest at G2/M phase and reactive oxygen species-dependent mitochondria-mediated apoptosis in non-small-cell lung cancer A549 cells, *Tumour Biol*, 39 (2017) 1010428317694565.
- [55] K. Yagi, Simple assay for the level of total lipid peroxides in serum or plasma, *Methods Mol Biol*, 108 (1998) 101-106.
- [56] V.K. Pulla, M. Alvala, D.S. Sriram, S. Viswanadha, D. Sriram, P. Yogeewari, Structure-based drug design of small molecule SIRT1 modulators to treat cancer and metabolic disorders, *J Mol Graph Model*, 52 (2014) 46-56.

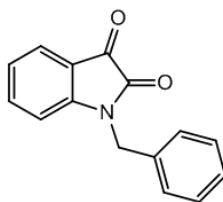
- [57] V.K. Pulla, D.S. Sriram, V. Soni, S. Viswanadha, D. Sriram, P. Yogeeswari, Targeting NAMPT for Therapeutic Intervention in Cancer and Inflammation: Structure-Based Drug Design and Biological Screening, *Chem Biol Drug Des*, 86 (2015) 881-894.
- [58] V.K. Pulla, D.S. Sriram, S. Viswanadha, D. Sriram, P. Yogeeswari, Energy-Based Pharmacophore and Three-Dimensional Quantitative Structure--Activity Relationship (3D-QSAR) Modeling Combined with Virtual Screening To Identify Novel Small-Molecule Inhibitors of Silent Mating-Type Information Regulation 2 Homologue 1 (SIRT1), *J Chem Inf Model*, 56 (2016) 173-187.
- [59] P.C. Rao, S. Begum, M.A. Jahromi, Z.H. Jahromi, S. Sriram, M. Sahai, Cytotoxicity of withasteroids: withametelin induces cell cycle arrest at G2/M phase and mitochondria-mediated apoptosis in non-small cell lung cancer A549 cells, *Tumour Biol*, 37 (2016) 12579-12587.
- [60] S.S. Dinavahi, S. Nyayapathy, Y. Perumal, S. Dharmarajan, S. Viswanadha, Combined inhibition of PDE4 and PI3Kdelta modulates the inflammatory component involved in the progression of chronic obstructive pulmonary disease, *Drug Res (Stuttg)*, 64 (2014) 214-219.
- [61] R. Gowda, S.S. Dinavahi, S. Iyer, S. Banerjee, R.I. Neves, C.R. Pameijer, G.P. Robertson, Nanoliposomal delivery of cytosolic phospholipase A2 inhibitor arachidonyl trimethyl ketone for melanoma treatment, *Nanomedicine*, 14 (2018) 863-873.
- [62] R. Gowda, G. Kardos, A. Sharma, S. Singh, G.P. Robertson, Nanoparticle-Based Celecoxib and Plumbagin for the Synergistic Treatment of Melanoma, *Mol Cancer Ther*, 16 (2017) 440-452.

Figure 1.

Isatin

ALDH1A1 IC₅₀ : 15.6 μ MALDH2 IC₅₀ : 16.9 μ MALDH3A1 IC₅₀ : 5.0 μ M

Cpd 3

ALDH1A1 IC₅₀ : 20 nMALDH2 IC₅₀ : 80 μ MALDH3A1 IC₅₀ : 7.7 μ M

KS99

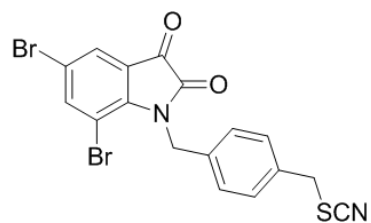
ALDH1A1 IC₅₀ : 350 nMALDH2 IC₅₀ : 1.5 μ MALDH3A1 IC₅₀ : 850 nM

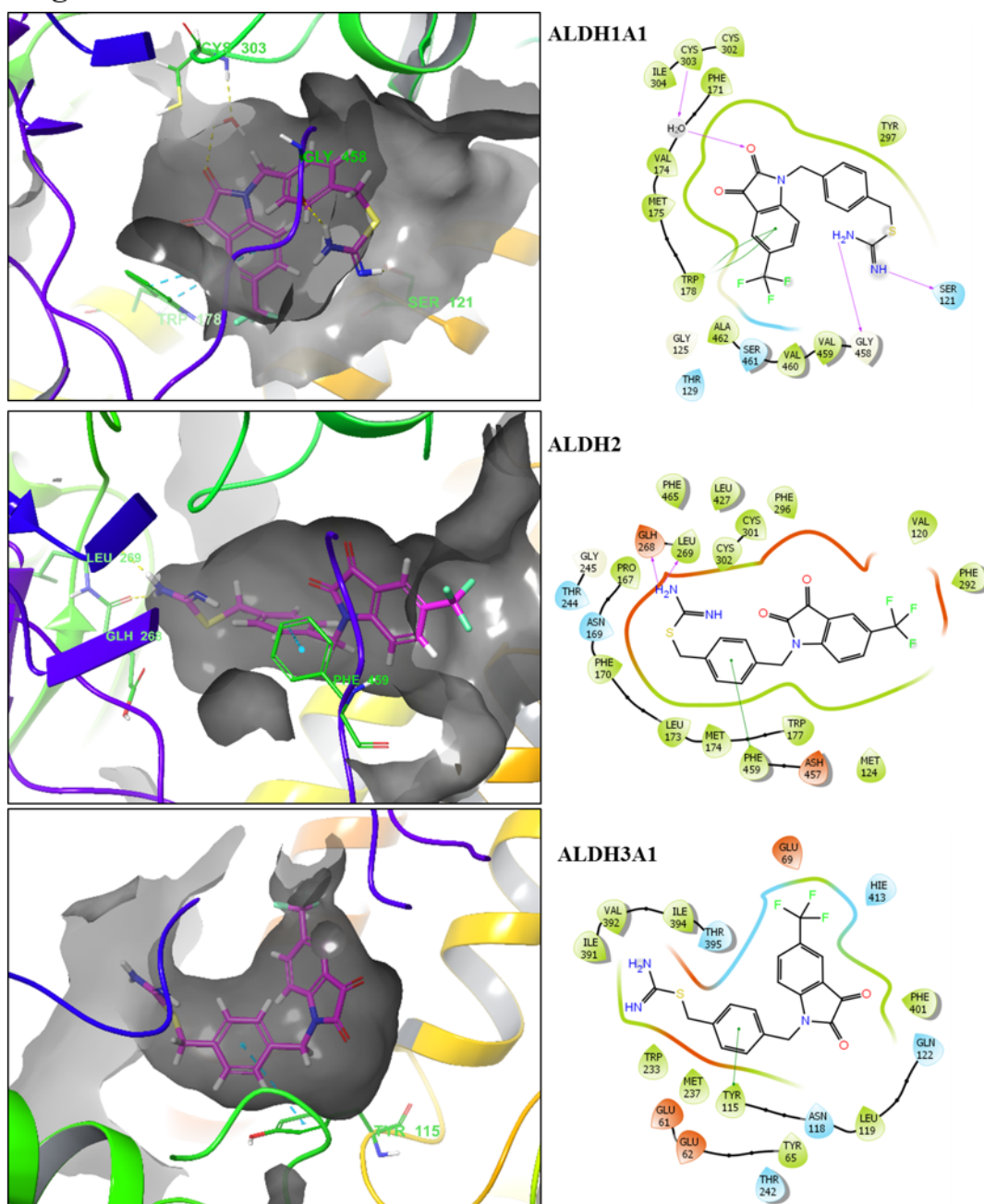
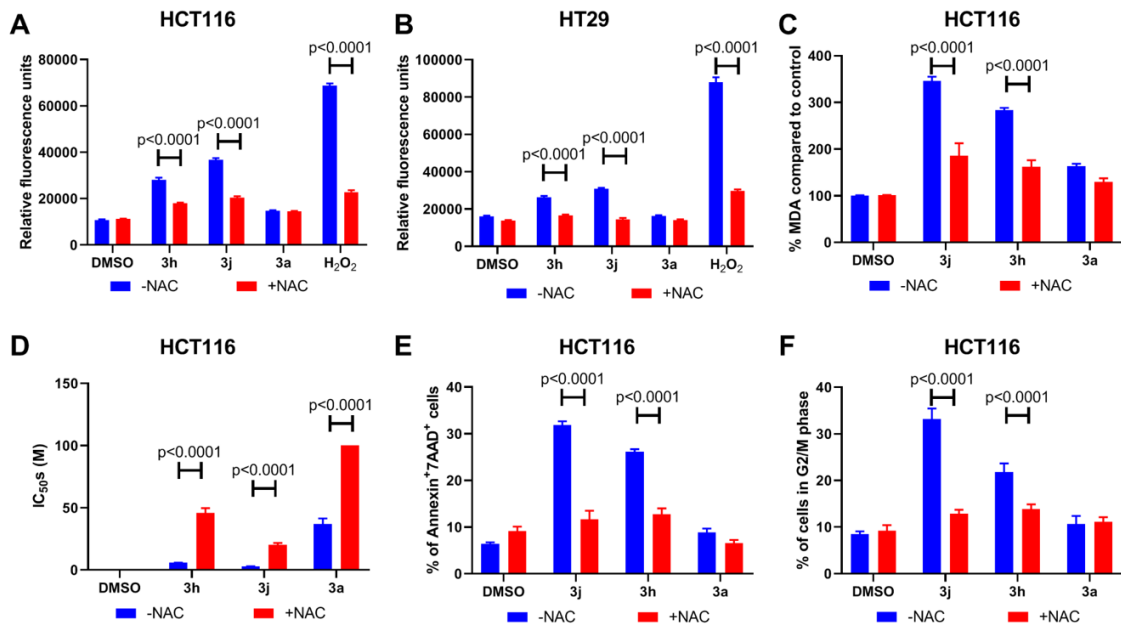
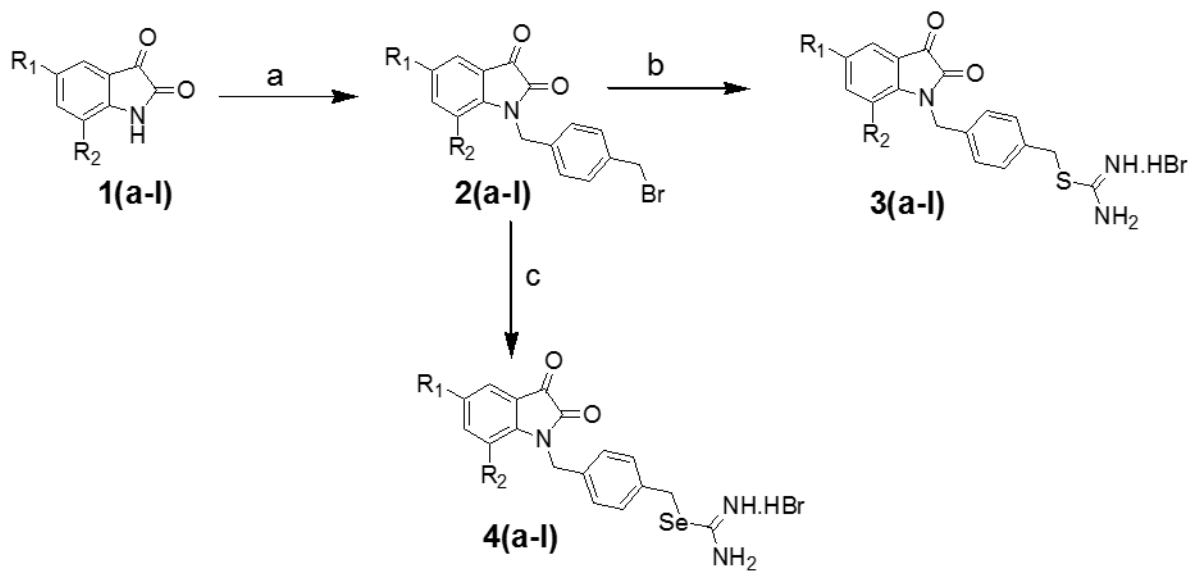
Figure 2.

Figure 3.



Scheme 1

Highlights:

- 24 derivatives were synthesized and tested for their ALDH1A1, ALDH2 and ALDH3A1 multi-isoform ALDH inhibitory activity.
- **3j** was the most potent multi-ALDH isoform inhibitor identified in the series with IC₅₀ of ALDH1A1 at 230 nM and ALDH3A1 at 193 nM.
- **3(h-l)** led to significant inhibition of cell proliferation in multiple cancer types.
- **3(h-l)** caused increased ROS activity, lipid peroxidation and toxic aldehyde accumulation and secondary to potent ALDH1A1, ALDH2 and ALDH3A1 inhibition.
- **3h** was the least toxic multi-isoform ALDH inhibitor *in vivo*.

Declaration of interests

The authors declare that they have no known competing financial interests or personal relationships that could have appeared to influence the work reported in this paper.